ENGINSOFT

futurities

Year 22
02
Summer
2025

The Simulation Based Engineering & Sciences Magazine

SPOTLIGHT

Excellence begins
with tolerance

- Editor’s Note

Welcome to the summer edition of Futurities, which turns the **Spotlight** on the topic of dimensioning and tolerancing, a subject of compelling significance in today’s environment of tough competition, tariff uncertainties and the related cost increases, and other geopolitical factors complicating material and component supply chains and cost. When there is so much that one cannot control, it makes practical sense to focus on what one can and, more importantly, those elements within one’s control that have the greatest impact on cost, manufacturability and functional performance, and this is where Geometric Dimensioning and Tolerancing (GD&T) comes into its own. In this section we look at the importance of dimension control in the production of medical devices, the often-overlooked aspect of model-based characteristics and the contribution they can make to GD&T, and we take a closer look at the ISO-GPS standard in the second article of our four-part miniseries on Tolerance and Measurement. We also touch on some of the training that is available on GD&T.

In this issue’s **Technology Transfer** section, we have an in-depth case study from the University of Padua concerning a comparison of approaches to the fatigue strength assessment of large, welded K-nodes in the offshore industry using MAGNA FEMFAT.

Our **Know-how** section includes an article from SPN Schwaben Präzision with tips for designing grease-lubricated gearboxes. Continuing the automotive theme, there is a contribution from the University of Rome “Tor Vergata” together with the Nissan Technical Centre Europe and RBF Morph, presented at the 2025 NAFEMS World Congress, which explores an innovative methodology to integrate styling, structural integrity and aerodynamic performance using Multiphysics optimization. The methodology is applied to wheel design for electric vehicles.

The **Research and Innovation** section turns its attention to the aeronautics sector with an article on the thermo-fluid dynamic simulation of hot isostatic pressure quenching (HIPQ) on aircraft blades. HIP is widely used by the aerospace sector for developing and producing alloys for high-performance applications such as turbine rotor blades. We also have a brief contribution from the EU-funded FF4EuroHPC project on a high-fidelity CFD workflow for optimizing wind-assisted propulsion systems, as well as news of the FFplus project’s second open call for business experiments for SMEs and startups.

Our **Product Peek** turns attention back to the automotive sector with an article from TSNE that describes the thermo-electrical analysis process of batteries using Ansys Mechanical and introduces the busbar thermal-electric analysis automation program.

This is decidedly an edition that is more mechanically focused, albeit looking at a multitude of facets and approaches to different aspects and applications of mechanical engineering. I hope you enjoy the read.

Stefano Odorizzi
Editor in chief

> “When there is so much that one cannot control, it makes practical sense to focus on what one can…

Futurities
Year 22 n°2 - Summer 2025

To receive a free copy of the next magazine, please contact our Marketing office at: marketing@enginsoft.com

EnginSoft S.p.A.
24126 BERGAMO c/o Parco Scientifico Tecnologico
Kilometro Rosso - Edificio A1, Via Stezzano 87 • Tel. +39 035 368711
50127 FIRENZE Via Panciatichi, 40 • Tel. +39 055 4376113
35129 PADOVA Via Giambellino, 7 • Tel. +39 049 7705311
72023 MESAGNE (BRINDISI) Via A. Murri, 2 - Z.I. • Tel. +39 0831 730194
38123 TRENTO fraz. Mattarello - Via della Stazione, 27 • Tel. +39 0461 915391
10093 COLLEGNO (TORINO) - Via Torino, 176 • Tel. +39 011 6525211

www.enginsoft.com
e-mail: info@enginsoft.com

Futurities is a quarterly magazine published by EnginSoft SpA

COMPANY INTERESTS
EnginSoft GmbH - Germany
EnginSoft UK - United Kingdom
EnginSoft Turkey - Turkey
EnginSoft USA
E-SOFT France
Particleworks Europe
www.enginsoft.com

CONSORZIO TCN www.consorziotcn.it • www.improve.it
M3E Mathematical Methods and Models for Engineering www.m3eweb.it
AnteMotion antemotion.com

ASSOCIATION INTERESTS
NAFEMS International www.nafems.it • www.nafems.org
TechNet Alliance www.technet-alliance.com

ADVERTISING
For advertising opportunities, please contact our Marketing office at: marketing@enginsoft.com

RESPONSIBLE DIRECTOR
Stefano Odorizzi

PRINTING
Grafiche Dalpiaz - Trento

Autorizzazione del Tribunale di Trento
n° 1353 RS di data 2/4/2008

Contents

TECHNOLOGY TRANSFER

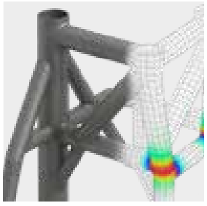

KNOW-HOW

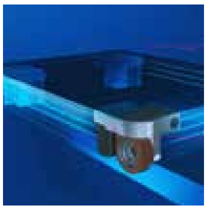

SPOTLIGHT

RESEARCH & INNOVATION

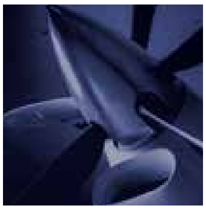

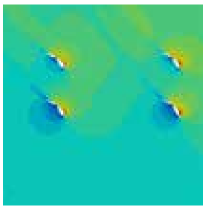

PRODUCT PEEKS

SPOTLIGHT

Excellence begins with tolerance

Holding the line: the role of tolerance in reliable design

Optimized tolerancing is not just a technicality; it reduces defects, saves money, ensures timely delivery, and improves brand reputation. It has a direct impact on product functionality, performance and producibility, but also on manufacturing costs and efficiency. Finding the right balance between dimensioning, dimension control and tolerance is therefore a strategic imperative for high-performing manufacturing operations. GD&T was created to ensure that tight tolerances are applied only where strictly necessary and that these can be clearly and simply communicated to all the players involved in the Product Development Process.

However, one of the key challenges is that it is considered too complicated to apply or is deemed necessary only for high-end products of advanced technicality. In reality, the opposite is true: it simplifies communication between all the various departments involved with a product, from design to production (machining and inspection teams). Ensuring a correct understanding and application of the discipline through training across all affected company departments helps reduce misunderstandings, rework, misapplication costs, and production delays.

This edition's **Spotlight** turns the focus on Tolerancing and Dimensioning with the second in our four-article mini-series on the topic, which focuses on the ISO GPS standard and its importance, as well as on some of the various dimensioning training available. The **Spotlight** also includes an article from Flex examining the role of mechanical variation management in medical devices through a case study on drug delivery devices. Finally, an article from Capvidia examines the vital, and frequently overlooked role, that model-based characteristics can play in GD&T.

The role of mechanical variation management in medical devices

A case study of drug delivery devices developed by Flex Health Solutions

by Enrico Boesso[1], Maurizio Volpe[2]
1. EnginSoft - 2. Flex Health Solutions

The development of medical devices presents unique challenges in terms of patient safety, regulatory compliance, technological innovation and the need for rigorous testing to ensure reliability and efficacy. These factors make the design and manufacturing process complex and require a multidisciplinary approach involving engineers, clinicians and regulators.

This applies to a wide range of devices, listed here by way of example, and which illustrate how challenging and unique work is in the medical sector, even though it shares pain points with products from other industries.

Types of medical devices:

- Diabetes care: testing and treatment equipment, personal monitoring devices, artificial pancreas
- Cardiovascular implants: implantable cardiac rhythm management devices, stents, surgical tools
- Diagnostics and testing: equipment for testing biological samples, molecular testing, genetic testing
- Orthopaedics: implants, surgical tools, surgical robots, endoscopy
- Life sciences: biological, molecular and genetic research equipment
- Gastrointestinal devices: surgical tools, surgical robots, biopsy harvesting devices, laparoscopic tools, endoscopy
- Urology: catheters, surgical tools
- Reproductive health: surgical robots, ultrasound devices, surgical tools, endoscopy
- Renal (kidneys) care: dialysis equipment
- Ear, nose and throat (ENT): scopes, surgical tools

- Oncology: radiation equipment
- Vascular devices: surgical robots
- Eye health: diagnostic and surgical tools
- Neurology: implantable neuromodulation devices, surgical tools, endoscopes
- General: infusion devices, surgical tools, robotic surgery and telemetry systems, endoscopes and viewing devices, non-invasive patient monitoring, anaesthesia systems, ventilators, needles
- Pharmaceuticals: drug delivery systems, inhalers, consumables manufacturing and testing equipment
- Patient management: medical beds, examination chairs, dental chairs, patient monitoring equipment
- Audiology: hearing aids, diagnostic equipment
- Cosmetic surgery: surgical tools
- Allergy solutions: diagnostics, vaccines

The reasons are easy to understand:

- Medical products require a responsible approach to product development to ensure product traceability and reliability: Due to the liability associated with medical devices, designers can be held accountable for every aspect of design, analysis, documentation, validation, and even component production.
- Product failure can have serious consequences: patient pain, and/or loss of life in the most severe cases. This can result in significant business impacts: major legal disputes or class actions inevitably impact corporate reputation.
- Competition for cheaper and more innovative solutions: Patents on medical devices have an expiration mechanism that allows competitors to enter the market as time passes. This makes it essential to be the first to patent solutions in order to tap into the initially high profit margins protected by the patent, and it is equally important to seek "cost-effective" product/process solutions once the patent expires in order to maintain a competitive advantage over new players entering the same market. For instance, patents for surgical robots began expiring in 2016 and were fully phased out by 2022. Potential competitors, both new and established, have been trying to enter the market with lower-cost offerings, some of which include partnerships with tech giants such as Google. There is, therefore, strong emphasis in the medical device sector on being first to market with pre-market approvals and patent applications.
- Customized, low-productivity, high-cost manufacturing and assembly processes because the problems these products must solve are often complex and multidisciplinary requiring the development of small parts and complex mechanical systems and/or intricate geometries that will fit inside the human body, and the use of inert materials that do not cause allergies/rejection by the body, all of which have a major impact on manufacturing and quality control processes. One cannot always rely on established manufacturing processes. In addition, the likelihood of production waste is significant, and it is extremely important that quality control is able to intercept any defective components.
- Manufacturers must overcome specific challenges in managing manufacturing and testing costs: parts that require unique materials and complex processes can be extremely expensive to manufacture and test and can have high scrap rates.
- Complex assembly processes can result in long production and delivery times. Extremely small parts and surfaces and uniquely shaped geometries can be difficult to inspect.

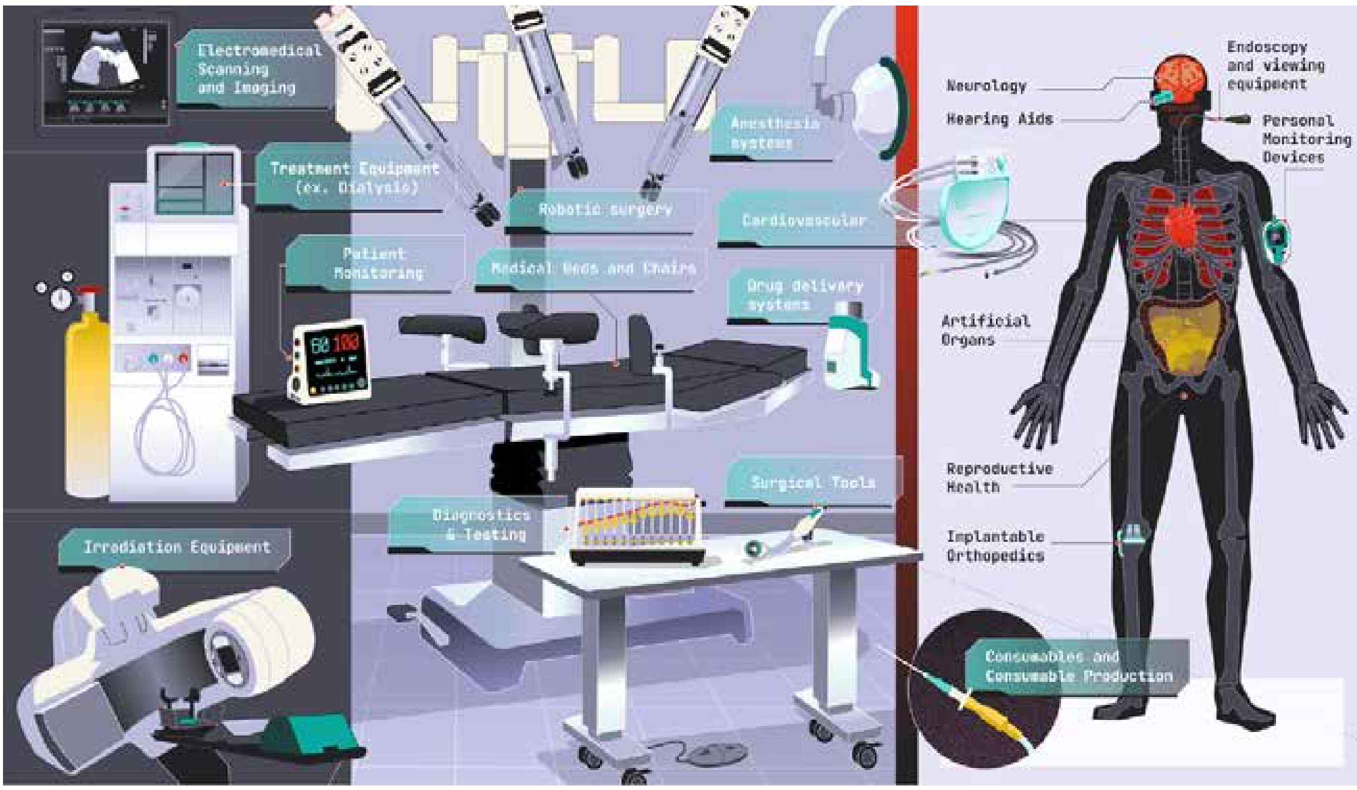

Clearly, these issues have a significant impact on the cost of product development itself.

Mechanical variation has a significant impact on all of the above. It is imperative that this impact is properly managed, monitored and documented.

What are mechanical variations and why do they impact these products so significantly?

All manufacturing processes inevitably produce "imperfect" products that deviate from the perfect nominal model, which only exists at the design level (3D CAD model). The actual geometry and/or size of all manufactured components will always deviate from the ideal counterpart. Therefore, to evaluate whether this deviation is acceptable and does not negatively affect the functionality of the final product to be assembled, it is necessary to introduce an acceptability criterion. This criterion is expressed in the technical drawings by assigning tolerance values to the various sources of geometric/dimensional variation. Once these tolerances have been defined, it is then possible to assess whether a component, produced by any manufacturing process, conforms to the requirements based on whether or not it conforms to the tolerances indicated on the drawing.

The evaluation of conformity involves making measurements on the manufactured parts. From a design and product development point of view, defining the tolerances to be included in the technical drawing is one of the most critical points because tolerances that are too wide negatively affect the quality and functionality of the product. Conversely, tolerances that are too tight increase the cost of manufacturing and testing components, with the risk of eroding profit margins once the product is on the market. It is therefore necessary to find a compromise between these two conflicting requirements. Mechanical Variation Management does just that.

What are the requirements for proper management of mechanical variation and its impact on the product?

Clearly, it is not just a matter of common sense. Several international regulations require the certification and pre-approval of medical devices before they can be placed on the market. Meeting the requirements of these regulatory frameworks is mandatory, otherwise the product will not be certified and cannot be marketed.

Regulatory oversight is required for most medical devices, particularly for Class III devices, which require full pre-market approval. Some of these regulations require the submission of detailed engineering studies that demonstrate that failure modes have been considered along with the variations in systems critical to their function. Some of these regulations include:

- FDA 21 CFR 820.30 and ISO 9001, clause 4.4 (www.fda.gov/media/116573/download). Page 25 of this document states that a tolerance stack should be performed as part of the design validation phase for complex systems or subsystems.
- FDA 501(k) (www.fda.gov/media/82395/download) discusses the criteria for approval. In 2014, the FDA issued revised 510K guidelines that refer to dimensions and design tolerances. This meant that medical device companies had to demonstrate that they had exercised due diligence on the potential impact of mechanical variation. Page 19 specifically mentions tolerances.

Specifically, how can mechanical variation management strategies be applied to product development?

These strategies can be applied to product development through dimensional management, an engineering methodology.

- Dimensional management promotes a continuous dialogue between designers, manufacturers, and inspectors of components through the exchange of information based on the geometric/dimensional requirements of the product, the "capability" of the various manufacturing processes (Pp, Cp, Cpk indices) to achieve the required precision, and the results of measurements made during dimensional inspection (scans, tomography, CMM, etc.). The aim is to find the best compromise solutions between often conflicting requirements.
- It uses predictive analysis (simulations) to anticipate and resolve potential product non-conformities before technical drawings are released to production, with a view to what is sometimes referred to as robust design (in this case, related to the geometric/dimensional domain).
- It is supported by measurement campaigns to evaluate the conformity of the manufactured parts with respect to the drawing requirements, and to monitor the behaviour of the production processes involved to identify potential savings in production costs and possible risks of drift in the stability of the production processes themselves.

Some tools are vital to successfully implement dimensional management.

Standardized technical language

It is essential to produce technical documentation that ensures unambiguous interpretation of the technical drawing. Today, this language is defined by international standards and regulations such as ISO-GPS (Geometric Product Specification) or ASME GD&T (Geometric Dimensioning & Tolerancing). Adopting such a language in technical drawings is not without its challenges: not only must designers and technical drafters be adequately trained to draw according to the rules of these standards, but those who receive the drawings must also be adequately educated about the implications from a manufacturing process and quality control perspective, including the impact on the hardware/software tools that must be used to verify the compliance of the components produced. The entire supply chain is certainly no exception in this regard.

Tolerance analysis

This is currently the only tool available to designers to evaluate tolerance widths and thus avoid under- or overestimating their impact on product quality. In fact, the analysis of the tolerance chain (stack-up analysis) makes it possible to anticipate the occurrence of potential non-conformities due to tolerances and their propagation, and to eliminate them before the product is industrialized, by means of real preventive corrective actions. Possible effects include increased productivity, greater repeatability of assembly processes (essential to avoid frequent stoppages of automatic lines), fewer production rejects, fewer non-conformities to manage and resolve, minimization of repairs/ rework, etc.

Tolerance analysis is often performed in the wrong context and using outdated calculation approaches. In terms of context, it is useful to remember the importance of performing these calculations before the components are manufactured: performing post-production checks to understand the extent of an out-of-tolerance impact that has already occurred is reductive and leads to little or no benefit in reducing cost or time to market. As far as calculation approaches are concerned, it is useful to emphasize that simplified calculation models are often used (the most common being the one-dimensional model of the "worst case") because they are extremely easy to apply (manual calculations or supported by electronic spreadsheets).

Such approximate models are mistakenly believed to be sufficient to obtain useful information for use in practice, only to be confronted with reality: simplified calculation models practically always produce results that are partly or completely unreliable, proposing tolerance values to include in the drawing that are so tight that they paradoxically make the product itself uneconomical (with production process costs higher than the sales price of the final product). It goes without saying that such tight values do not represent the real functional requirements of the product but are derived from an inherently overly cautious calculation approach.

These considerations also form the basis of the widely held perception that tolerance analysis is of little use in product development: why should I spend time and resources developing calculation models that have marginal (or no) impact in practice? The reality is that tolerance analysis is fundamental and has potentially very significant impact. The only way to make it truly useful is to get it right. Calculation models must therefore represent reality to produce reliable results that can be used to support decisions.

Reality is three-dimensional: chains always contain dimensional and geometric tolerances; these tolerances have error-amplifying effects in 3D; the real behaviour must be described by variables that are probability distributions (statistical models), etc. In short, you cannot deal with such complexity by imposing hugely influential simplifying assumptions on calculation models! The complexity makes it impossible to conduct tolerance analyses manually: dedicated software such as CAT (Computer Aided Tolerancing) facilitates the work, allowing analysts to perform very complex 3D analyses with statistical variables in a relatively simple manner and within an acceptable timeframe for today's development times.

Some further considerations on implementing Dimensional Management models

Bottom-up initiatives are often proposed: designers, engineering, and R&D feel the need to "do something" to manage tolerances and try to make do with what is available. Such attempts are almost always doomed to failure because they underestimate the problem.

Many believe that it is sufficient to make ISO-GPS compliant drawings and do tolerance chain calculations; it is not. This "compartmentalized" way of working is often counterproductive and creates more problems than it solves. In fact, one must remember that the technical drawing "travels" during the product development process, ending up in the hands of those who must produce the product, and afterwards in the hands of those who must check the component. Can you be certain that the people who receive the drawing can read, understand and interpret it correctly? Are you certain that they have the hardware and software tools to collect and process data compliantly with international standards?

When looking at the problem from an organizational perspective, it is not sufficient to perform the assigned task within the engineering office alone. Rather, the problem must be tackled in its entirety and complexity, considering all potential interactions.

The emblematic example is procurement: if the engineering department adopts ISO-GPS technical language for producing engineering drawings, one of the criteria for qualifying new potential suppliers (or auditing existing suppliers) must be based on their ability to process this type of information. It seems trivial, but all too often these considerations are completely ignored.

For all these reasons, it is extremely important that the managment executives of companies are made aware of the issue and understand its potential impact on the business. In fact, they should be the ones to support and promote dimensional management initiatives within companies with a top-down approach, knowing that to achieve concrete (economic) results requires staff training, the adoption of appropriate tools (investments), and redefinition/ control of business processes.

Flex Health Solutions case study: drug delivery device

Drug delivery devices, which are devices specially designed and developed to enable the dosage and subsequent administration by injection of drugs such as insulin for the treatment of diabetes,

or the latest generation of drugs to treat obesity.
These devies can be purely mechanical (i.e. with springs) or electrical, where the actuators are managed by software. They are portable and must meet requirements for ease of use, accuracy of dose delivery and, of course, cost.

Therefore, the precision of the components, miniaturization and electrical consumption for the duration of any batteries are of fundamental importance. From a mechanical point of view, these devices can be compared to a plastic resin CNC machine the size of a smartphone.

Dimensional Management as described in this paper has been successfully implemented by Flex Health Solutions over the last few years, along with the use of ISO-GPS technical language in its technical drawings, and the dissemination of skills to independently perform complex

Fig. 1. Technology demonstrator of an autoinjector. This is not an actual product.

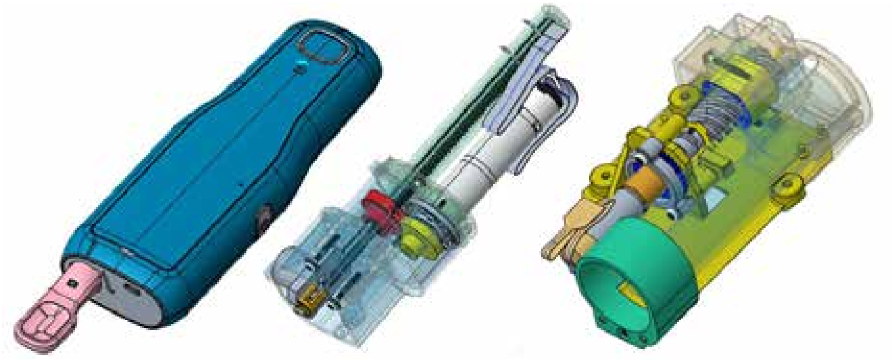

Fig. 2. Technology demonstrator of an autoinjector - CAD model.

tolerance analyses using CAT Cetol 6σ software from Sigmetrix. Throughout this process, EnginSoft has played an important and continuous role, not only supplying the software, but also providing various face-to-face training sessions for Flex Health Solutions staff at the company's Milan facility, and consulting activities. This has made it possible to achieve concrete results to support product and process improvement decisions.
The identification of the dimensions to be included in the drawings of mechanical components follows a process that starts from the functions that the component must perform and the iterations that it has with the other components.

This "functional" approach to the identification of dimensions implies a wide use of geometric tolerances for the definition of component specifications and has been made possible by:

- implementing a rigorous dimensional management system using the ISO/GPS standard;
- using new prediction tools such as Sigmetrix Cetol 6σ and verification tools such as computed tomography.

This has allowed us to identify and focus only on the really important dimensions that have a functional impact, with the

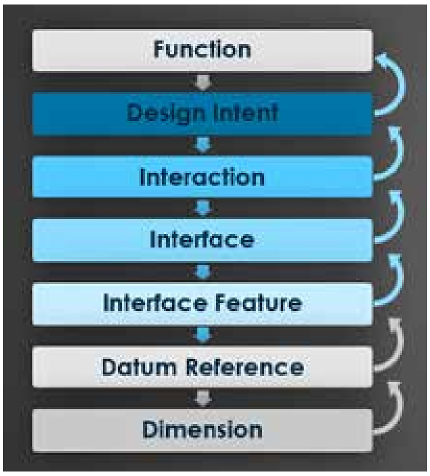

Fig.3. Design process that illustrates the link between functions and feature dimensions.

double benefit of improving quality by predicting the impact of tolerances and reducing production costs by requiring dimensional checks only where necessary and relaxing them elsewhere.

"The use of Cetol allowed us to identify the most critical dimensions to meet the requirements and, thanks to the complete integration with CREO, this was done in real time from the design phase", declared Maurizio Volpe, Mechanical Engineering Manager at Flex Health Solutions.

For more information:
Enrico Boesso – EnginSoft
e.boesso@enginsoft.com

About Flex

Flex is the manufacturing partner of choice, helping a diverse customer base design and build products that make the world a better place. With the collective strength of a global workforce in 30 countries and responsible, sustainable operations, Flex delivers technology innovation, supply chain, and manufacturing solutions to various industries and end markets.

Model-based characteristics: the missing link in dimensional management

by Jimmy Nguyen
Capvidia

For decades, engineering teams have relied on drawings, and, more recently, 3D product manufacturing information (PMI) to communicate the critical dimensions and tolerances a part must meet.

However, spreadsheets and balloons on PDFs still creep in whenever the quality or manufacturing team needs to create an inspection plan or a first-article report. These hand-offs introduce risk: data can be re-typed, mis-interpreted, or become orphaned from its original context. Siemens' new model-based characteristics (MBC) capability in NX Inspector eliminates this risk by converting every tolerance requirement into a traceable, standards-compliant data object that accompanies the model from design to the shop floor.

What exactly is a model-based characteristic?

In a model-based definition, a characteristic is the smallest, machine-readable requirement that quality control or manufacturing must verify on a part. Each piece of product and manufacturing information (PMI) can be broken down into several characteristics. For instance, a single hole call-out may result in separate items for diameter, thread pitch, positional tolerance, and surface finish. Since models can contain dozens or even thousands of features, the same PMI note may generate repeating characteristics for each instance of a feature or entirely different ones when the design requires it.

Treating these requirements as discrete, uniquely identified data objects is more than just tidy bookkeeping. It enables downstream systems to perform their tasks automatically. NX Inspector now allows users to create these characteristics directly within the CAD session, assign them unique IDs, and store their semantics according to the Digital Metrology Standards Consortium (DMSC) specification. This is the first CAD-native implementation of the DMSC MBC standard. Because it conforms to an open standard, the data can be exported to neutral formats, such as QIF or PLMXML, for use in any downstream CMM, CAM, or MES system. Closing the model-based definition loop

With characteristics authored, stored, and exchanged in a consistent, standards-compliant format like QIF, NX supports bidirectional interoperability and traceability with robust MBD software programs such as Capvidia's MBDVidia. Model data can be validated, enriched, and returned, facilitating true closed-loop feedback between design, quality, and manufacturing. Machine-readable data can be ingested directly downstream, enabling a true model-based enterprise (MBE). MBDVidia automates inspection planning, first article inspection (FAI) reports, and metrology workflows, eliminating the need for manual ballooning, spreadsheet re-entry, or loss of context.

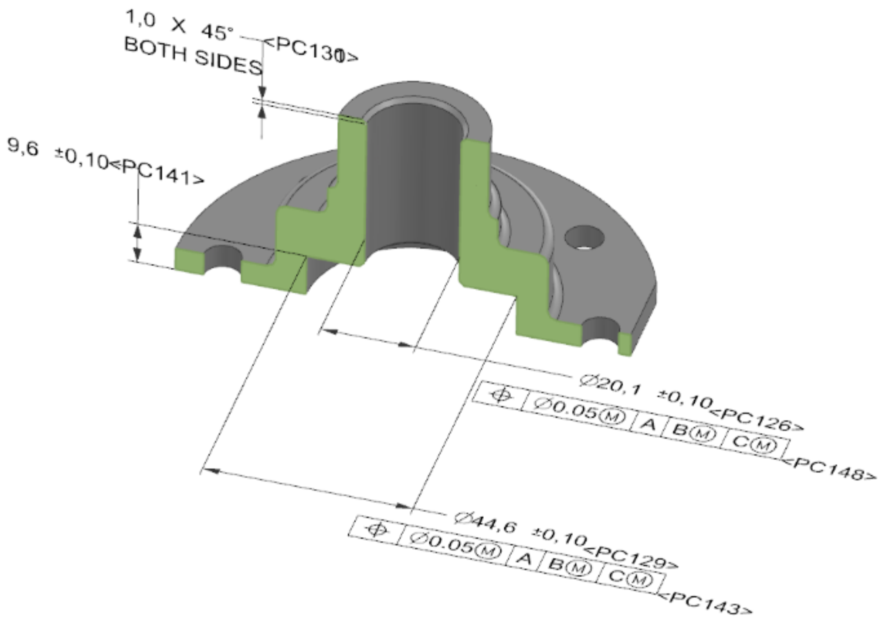

Fig. 1. NX is the first major CAD native to implement model-based characteristics (Source: Siemens Digital Industries Software - blogs.sw.siemens.com/nx-design/whats-new-in-nx-nx-inspector-and-mbd/)

The result is a clean digital thread extending from design to manufacturing to metrology, which eliminates re-typing errors, preserves traceability, and accelerates first-article and in-process inspections. Upstream intelligence guarantees that validated, enriched QIF data flows back into NX, thereby improving product quality and enabling true design-for-inspection.

Key benefits of the NX–MBDVidia integration:

- Downstream automation: MBDVidia automates inspection planning, FAI reports, and metrology workflows using NX-generated QIF data, reducing manual rework and setup time.
- Upstream intelligence: MBDVidia sends validated, enriched QIF data back into NX to improve product quality and enable design-for-inspection.
- Cross-CAD interoperability: MBDVidia supports native MBD across Siemens' NX, PTC Creo, SOLIDWORKS, and Autodesk Inventor to ensure full compatibility among design, quality, and manufacturing systems.

Robust MBD has always aimed to connect design intent to manufacturing reality without detouring through drawings. By converting design intent (PMI) into accountable requirements (MBC), NX Inspector and MBDVidia finally close that loop.

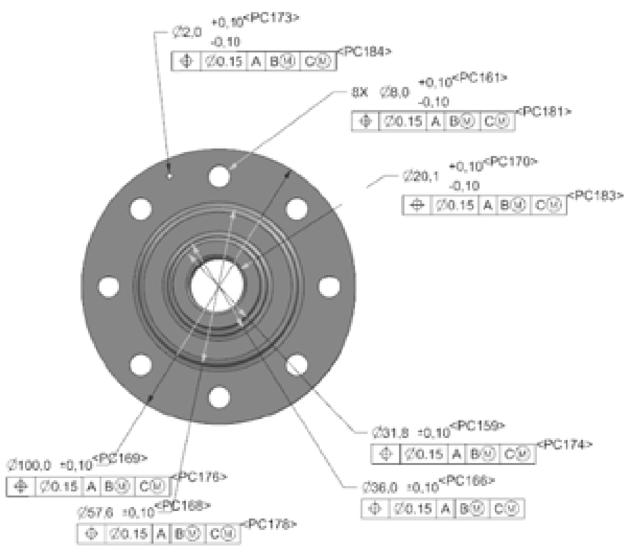

Fig. 2. Model-based characteristics are machine-readable quality and manufacturing requirements consumed downstream automatically by CAM and CMM (Source: Siemens Digital Industries Software - blogs.sw.siemens.com/nx-design/whats-new-in-nx-nx-inspector-and-mbd/)

About Capvidia - Leading innovation

Founded in 1994, Capvidia has been at the forefront of emerging technologies in manufacturing. The company was the first to market with CAD translation in 2000 and first to market with CAD validation for Boeing validation in 2009.
In 2013, Capvidia saw the confluence of high-speed internet, fast computing, big data, and cyber-physical technologies to create conditions for a true quality-based digital thread throughout the product lifecycle. The company bet on model-based workflows as the future of manufacturing.

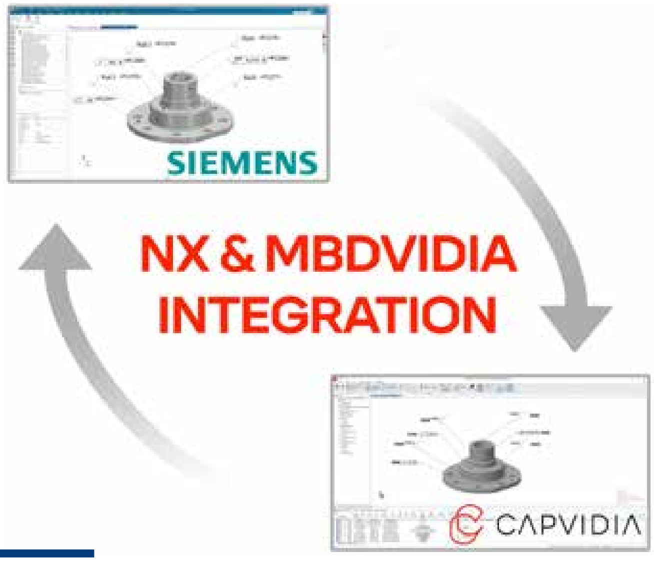

fig. 3. NX and MBDVidia integration automates quality workflows downstream and sends validated, results data back to NX (Source: BusinessWire.com - businesswire.com/news/home/20250609650970/en/Capvidia-Expands-Model-Based-Definition-MBD-Interoperability-with-QIF-Enabled-NX-Software)

Why it matters for tolerance and dimensional management

Dimensional management involves more than selecting the appropriate GD&T symbols. It also involves maintaining intent, accountability, and proof of conformance throughout every stage of the product lifecycle. Traditional drawing balloons and Excel spreadsheets are fragile; one missed revision or typo can invalidate an entire batch. Model-based characteristics offer:

- Consistency – A single standards-based schema governs the definition and use of all feature requirements.
- Traceability – UUIDs and PLM history connect CAD, BoC, and measurement data enabling quick root-cause analysis.
- Automation – Associative updates and rule-driven ballooning eliminate the need for manual data re-entry.
- Interoperability – Neutral exports (QIF, PLMXML) allow any metrology software to operate within the same digital thread.

These benefits transform tolerance control from a paperwork exercise into a data-driven, closed-loop process.

Takeaway

Model-based characteristics transform PMI from visual annotations into actionable, auditable data. Embedding every tolerance as a standards-compliant object and integrating it into PLM, manufacturing, and quality processes fulfils the initial promise of model-based definition: providing a single, authoritative source of dimensional truth that accompanies the product throughout its entire lifecycle.

For more information:
Jimmy Nguyen, Brand Manager, Capvidia
jimmy@capvidia.com

TOLERANCING MINI-SERIES

Tolerances are a fundamental part of modern product design and manufacturing. They affect not only the quality and performance of a product, but also its cost, manufacturability and time-to-market. Poorly defined tolerances, inadequate reference patterns, or inefficient assembly sequences can lead to high production costs, higher rework and scrap rates, and delays in product launch. It is therefore critical for engineering organizations to have a clear understanding of the impact of tolerance decisions throughout the product development process (PDP).

In today's increasingly complex and multi-functional design environments, tolerances must be precisely defined, managed, and communicated. This ensures that critical dimensional information flows seamlessly from design to production to quality control, and back to engineering. Whether documented in 2D engineering drawings or incorporated into 3D CAD master files, tolerances and reference structures are the backbone of design intent and product quality assurance.

This series of articles explores four key aspects of modern tolerance:

1. Dimensional Management (DM)
2. ISO GPS – Geometrical Product Specifications
3. Statistical Simulation of 3D Tolerance
4. QIF format for model-based definition (MBD) and digital continuity

Each article aims to provide insights into how tolerance can be systematically implemented in PDP, using simulation, standards, and digital tools to improve product quality and reduce manufacturing costs.

Definition of Geometric Dimensioning and Tolerancing in ISO GPS

by Florian Weidenhiller
EnginSoft Germany

The definition of tolerances according to the ISO GPS standard is central to modern dimensional management. Building on the principles of deriving tolerances and references from product and assembly requirements, as presented in the first part of this article, this section focuses on the practical implementation of ISO GPS – the international series of standards for geometric product specification.

Basics: the functional definition of datum reference frames (DRFs)

Component tolerances are fundamentally defined based on the assigned functional reference system. DRFs are specified in ISO 5459 and are based on how the component functions within the overall product. They are defined by the six degrees of freedom (translation and rotation axes of the component). The following principle applies: DRFs are derived from the geometric assembly elements of the component as well as the sequence in which they are aligned during the assembly process.

Typical functional geometries include planar surfaces, holes, pins and spherical surfaces i.e. geometries that are suitable for achieving stable and reproducible alignment of components. These "standard geometries" are documented on the drawing as DRFs in accordance with ISO GPS and form the binding basis for production, assembly, testing, and quality control.

Defining the degrees of freedom (DOFs)

When determining the DRFs, the role of each geometric element in limiting certain DOFs must be considered. For example, a reference plane defines three DOFs (translations in the normal direction, and rotations around the two main axes of the plane).

Conversely, a borehole or shaft with predominantly axial alignment defines four DOFs (two x translations and two x rotations perpendicular to the main axis).

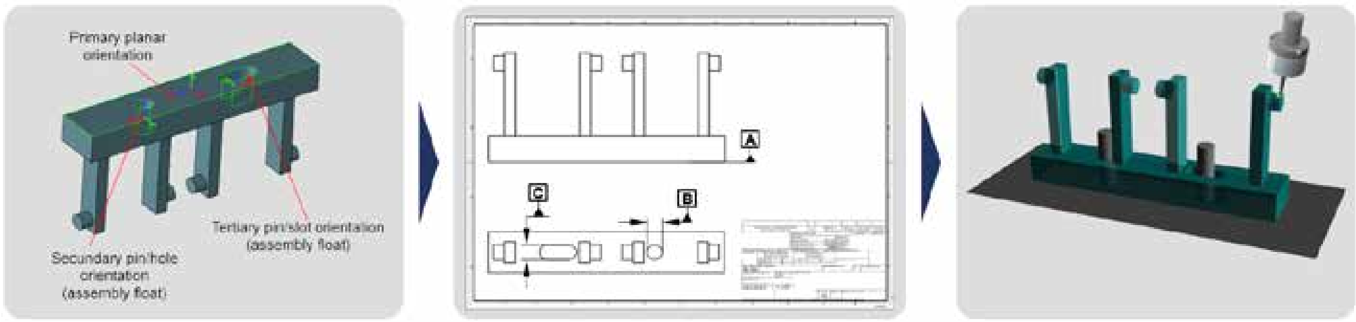

Fig. 1. Derivation of part and measurement DRF from assembly orientation.

The sequence of these constraints is not arbitrary: in the so-called "primary-secondary-tertiary" principle, the most important surface or axis is defined first (primary datum), followed by additional references to fully constrain all six DOFs.

Top-down approach: consistency of DRFs

A fundamental principle of the ISO GPS approach is to ensure consistency of DRFs at all assembly levels, from the final product to its individual components. This top-down approach ensures that the DRFs of the components align with the reference system of the final product.
However, "DRF flaws" can arise when new or different DRFs are defined in subassemblies or individual components. This can lead to unwanted variation accumulations, assembly problems, or quality deviations. The solution: DRF elements are derived from the top-level assembly and inherited across all sub-levels.

Geometric tolerances in relation to DRFs

Once the DRFs have been clearly defined, the tolerance definitions will be established in accordance with the ISO GPS series of standards, including ISO 8015, ISO 17450 (Basic standards), ISO 5459 (DRF), ISO 1101 (form, location, orientation and runout) and ISO 5458 (pattern tolerancing). The following distinctions are made:

- Position tolerances define the position of an element in relation to a DRF
- Profile tolerances regulate permissible deviations of surfaces or planes (e.g. surface profile, or line)
- Orientation tolerances limit rotational deviations (e.g. perpendicularity, angularity, and parallelism)
- Form tolerances describe a single geometric element (e.g. straightness, flatness, roundness, cylindricity, or a profile without datums)

In this context, position and profile tolerances warrant particular attention, as they cover form, position and orientation. These tolerances serve as "master tolerances" for numerous function-critical elements.

The specific tolerance values depend on the function of the element within the product, the material used, the manufacturing process, and environmental factors such as temperature and humidity.

Training and qualification of ISO GPS standards

Implementing the ISO GPS standard in practice requires a solid knowledge base. Therefore, it is critical to the success of the project that all the developers, designers, quality, and production experts involved receive training.

EnginSoft's basic ISO GPS training courses typically last two days and cover the methodology for defining DRFs, as well as how to interpret and apply tolerance symbols. Advanced training courses and customer-specific workshops are also available. During these courses, components in technical drawings are analysed according to their function and specific tolerances are derived.

The ISO GPS CBT (computer-based training) course from Sigmetrix provides flexible, location- and time-independent training. Spanning 13 chapters and approximately eight hours, this course provides all areas of a company with the necessary basic knowledge. An added benefit of the CBT is that it is permanently available as a digital knowledge base that can be revisited as required.

Conclusion

Rather than being an isolated step at the end of the design process prior to releasing technical drawings, defining geometrical dimensions and tolerances is an integral part of systematic tolerance management. Functional definition of references, use of consistent DRFs throughout the product, and targeted training of those involved ensure cost-optimized components, product quality that meets ISO GPS standards, and reproducible, high performance production processes.

For more information:
Enrico Boesso – EnginSoft
e.boesso@enginsoft.com
and Florian Weidenhiller
EnginSoft Germany for DACH region
f.weidenhiller@enginsoft.com

BOSCH

Invented for life

Smart digital learning is transforming skill development at Bosch.

With the ISO GPS CBT from Sigmetrix, we ensure our associates worldwide stay up to date with the latest ISO GPS standards.

This digital learning solution enables just-in-time re- and upskilling—when and where it's needed.

Its flexible, on-demand approach empowers our teams in research and development, production, quality assurance, and technical purchasing to stay ahead in a rapidly evolving business landscape.

Simon Schmitt
Senior Product Manager Corporate Learning
at Bosch Training Center

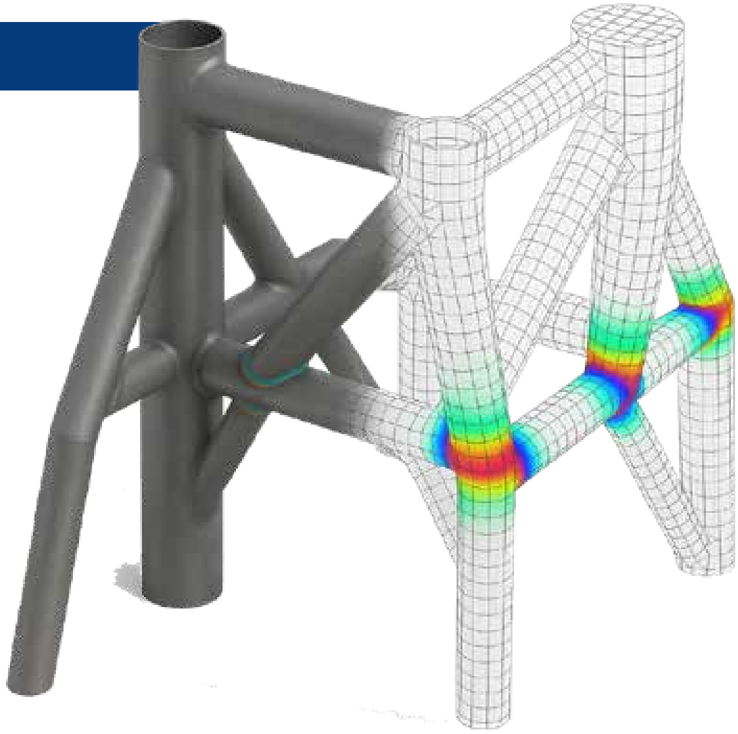

Fatigue strength assessment of large welded K-nodes in the offshore industry: a comparison of approaches using MAGNA FEMFAT software

by Alberto Visentin and Giovanni Meneghetti
Department of Industrial Engineering, University of Padua

When it comes to the fatigue design and durability assessment of modern welded engineering structures, mechanical engineers are faced with the dual challenge of large-scale complex geometries and constant and time-varying real-world loads. The most common approach is to use methods based on nominal stresses, as set out in international standards and recommendations. These approaches allow analysts to calculate the nominal linear-elastic stresses acting on a welded component using simple solid mechanics formulas, regardless of the weld's geometry. The calculated stress must then be compared with the fatigue strength of a suitably classified structural detail, depending on its geometry and loading conditions.

Standards provide a wide range of references for fatigue designs, which are commonly known as "FAT" classes. These are valid for the most common welded components encountered in engineering practice. However, the standards do not always provide the appropriate classified details for complex geometries and multi-axial loading conditions. Finite element (FE)-assisted *approaches*, such as the hot-spot and *notch stress* methods, have been shown to reliably complement the popular nominal stress method. Nevertheless, in some circumstances, advanced methods for the fatigue design of welded structures, such as the *notch stress approach*, may require the following:

1. time-consuming pre-processing procedures to accurately model the detailed geometry of welds.
2. significant computing resources to solve FE models with locally refined meshes near the welds; and
3. manual routines to post-process FE stress results in order to evaluate the fatigue strength of welds.

With this in mind, it is clear that evaluating the fatigue strength of large welded structures can be challenging in terms of time, computing resources and the qualified personnel required for finite element analysis. These challenges are commonly encountered in sectors such as amusement park structures, automotive design, offshore structures, mining and earth-moving, and agriculture vehicles and equipment. This prompts companies to look for simplified analysis techniques that provide reliable results quickly.

In this context, the value of commercial fatigue analysis tools lies in their ability to automate the application of well-established methods, thereby reducing the time and effort required for post-processing FE-calculated stresses and performing fatigue durability estimates.

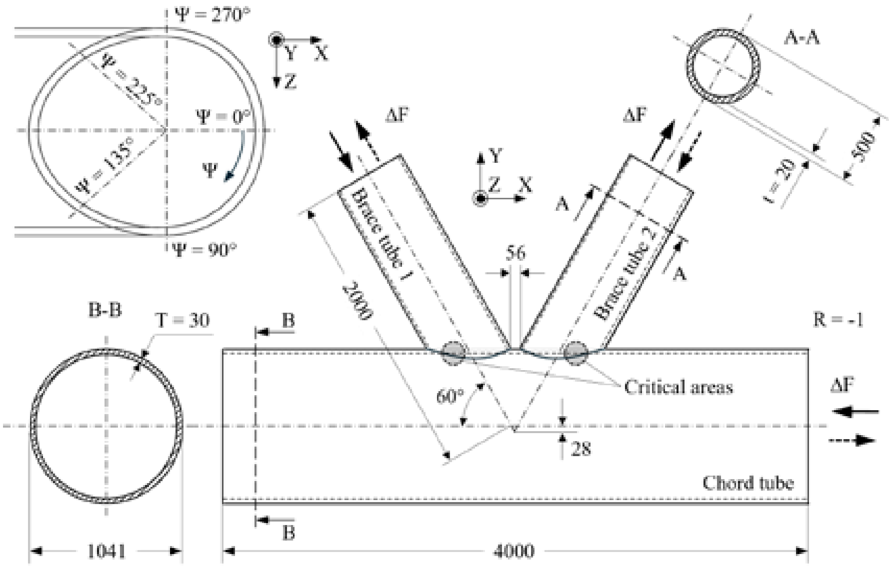

Fig. 1. Geometry of welded K-nodes. The dimensions shown are in millimetres.

Introduction

This study used the MAGNA FEMFAT commercial software to assess the fatigue strength of large welded K-nodes, which are commonly used on small offshore platforms. Firstly, three different FE models of a real large K-node were developed in Ansys Mechanical using 3D *shell* and 3D *solid* finite elements. The FEMFAT fatigue analysis tool was then used to post-process the extracted stress results from the Ansys finite element analyses in order to estimate fatigue durability. Three fatigue analysis approaches implemented in FEMFAT (the *Shell* WELD approach, the *Solid*WELD approach, and the R1MS approach) were then compared. A set of experimental data from the literature relevant to the fatigue strength of the welded K-nodes under investigation was considered and re-evaluated. Finally, the number of cycles to crack initiation in experimental fatigue failures was compared with the fatigue life estimates made using the S-N fatigue design curves implemented in FEMFAT.

Large K-joints for the offshore industry

C. M. Sonsino [1–3] investigated the fatigue strength of large, welded K-joints made of E355 fine-grained structural steel under normalized conditions ($\sigma_{Y0.2} \geq 355MPa$ and $\sigma_U \geq 470MPa$ in [1]). The welded specimen consisted of two diagonal tubular braces, each with a diameter of 500mm and a thickness of 20mm. The braces were joined to a chord tube with a diameter of 1,041mm, a thickness of 30mm, and a length of 4,000mm at a 60-degree angle of incidence (see Fig.1). A full-penetration welded connection was achieved between the ends of the brace tube and its surface using conventional multi-layer welding. During the joining process, a 56mm gap was generated between the two braces (see [1]).

Experimental fatigue tests were performed with constant and variable amplitude loads using a dedicated test rig equipped with a servo-hydraulic actuator with a maximum load capacity of 2,500kN. The actuator was connected to the chord, and the applied horizontal load was transmitted to the braces via longitudinal bars [3]. As a result, the braces tubes experienced fully reversed axial loads, while the chord tube experienced a unidirectional tensile-compressive axial load with a load ratio of $R = -1$ [1–3].

A total of eight specimens were tested for fatigue resistance in an artificially generated seawater environment (see Table 1). The seawater was continuously aerated and circulated around the welds, and no corrosion protection was applied [1]. Three specimens underwent fatigue testing with constant amplitude (CA) loads and five specimens underwent fatigue testing with variable amplitude (VA) loads using a standard relative load spectrum (or stress amplitude) derived from wave loads in the North Sea [1–3]. Fig. 2 shows this spectrum, characterized by a spectrum factor of 1.0 (i.e. linear in a log-linear diagram) and a length of $L_s = 5{\cdot}10^6$ cycles. According to the COLOS (Common Load Sequence) standard [1], this corresponds to an operating time of one year.

As stated in [1], all stress amplitudes below 15% were omitted to achieve reasonable test periods. Moreover, it is assumed that fatigue damage is primarily caused by high stress amplitudes while lower stresses do not significantly contribute to the damage process [1]. Modifying the original spectrum produced a reduced spectrum with a spectrum length of $L_s = 4.94{\cdot}10^5$ cycles and a p-factor of 0.15. Here, p is the ratio of the minimum to maximum stress amplitude in the spectrum.

Fatigue loads were applied repeatedly until fatigue cracks initiated at the weld toe of the chord near the saddle points of braces 1 and 2 (see Fig. 1), at an angular position of

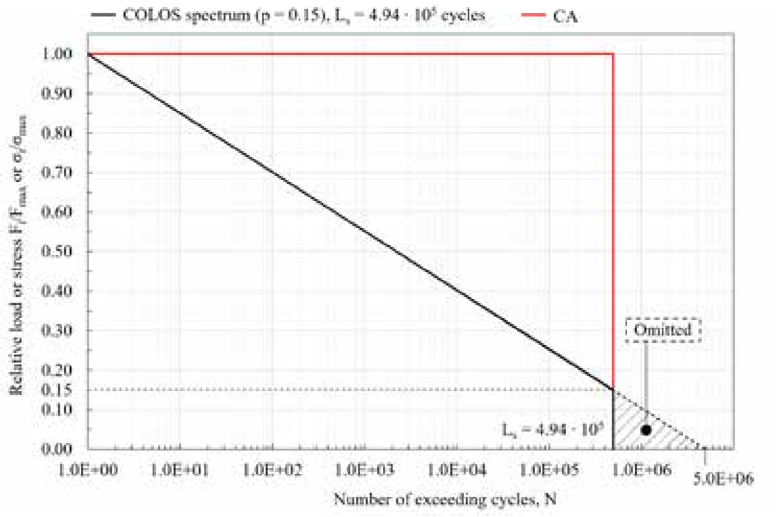

Fig. 2. In accordance with the COLOS (Common Load Sequence), the standard North Sea wave load spectrum is used for load configurations with variable amplitude (VA) [3].

Specimen No.	Load range ΔF_{max} [MN] *	Stress amplitude scale factor f_s ^	Crack initiation N_{init} [cycles]	Breakthrough N_{bt} [cycles]	Site of crack initiation	
					Ψ (°)	Brace
6, CA	1.50	1.07	$1.60 \cdot 10^5$	$3.95 \cdot 10^5$	90	1
7a, CA	1.00	0.71	$6.00 \cdot 10^5$	$1.92 \cdot 10^6$	105	1
7b, CA	1.00	0.71	$8.05 \cdot 10^5$	$1.92 \cdot 10^6$	270	1
1, VA	3.00	2.14	$5.93 \cdot 10^5$	$2.22 \cdot 10^6$	90	2
10, VA	3.00	2.14	$8.00 \cdot 10^5$	$3.96 \cdot 10^6$	225	1
13, VA	1.70	1.21	$7.42 \cdot 10^5$	$1.46 \cdot 10^7$	120	1
3, VA	2.00	1.43	$2.82 \cdot 10^6$	$1.29 \cdot 10^7$	120, 135	1,2
2, VA	2.00	1.43	$1.20 \cdot 10^5$	$6.30 \cdot 10^6$	90	1

** Maximum load range applied in experimental fatigue tests.*
^ Stress amplitude scaling factor, according to Eq. (2), is used to linearly scale the stress amplitude results calculated using FEM.

Table 1. Relevant experimental fatigue results for K-nodes tested under constant and variable amplitude loading.

approximately 0–45° from the saddle point (i.e. $\Psi = 90 \div 135°$, see Table 1). The fatigue life at crack initiation was defined by assuming a technical crack with a depth of 1mm and a surface extension of $2l = 20mm$, as measured using potential-drop techniques. Subsequently, the fatigue cracks propagated through the chord tube, and the total fatigue life was defined as the number of cycles to breakthrough (failure) [1–3].

FE fatigue strength assessment using shell and solid FE models

The fatigue strength of the welded K-node in Fig. 1 was investigated numerically using the MAGNA FEMFAT fatigue analysis tool. The following approaches were considered for comparison purposes:

(i) The FEMFAT Shell WELD approach requires an FE model solved using linear or quadratic shell finite elements as input. This approach does not model the detailed geometry of the welds and recommends a maximum element edge length of twice the plate thickness to provide sufficient mesh refinement for calculating structural stresses. Nodes and elements that share the seam line between the joining plates — referred as *"weld nodes"* and *"weld elements"* — can be saved in *named selections* so that FEMFAT can easily locate them.

(ii) The FEMFAT *Solid*WELD approach requires an FE model solved using quadratic *solid* finite elements. The detailed geometry of the welds must be included in the model. Rather than modelling the weld toes and weld roots with rounded edges and roots, they should be modelled as sharp V-notches. The FE mesh should be locally refined around the profile of the welds, providing at least three elements across the sheet metal thickness. This should be done while ensuring that the maximum size of the finite elements is $1 \div 2mm$. When creating the input FE model, the nodes belonging to the weld toe and weld root should be stored in *named selections* according to the nomenclature set out in the FEMFAT guidelines.

(iii) The FEMFAT R1MS approach requires am FE model that has been solved and generated using quadratic solid finite elements. The model must include the detailed geometry of the welds. Additionally, a notch radius should be introduced at the weld toe and weld root. According to the FEMFAT guidelines, the notch radius at the weld toe should be 1mm for thicknesses greater than 5mm. On the other hand, the notch radius should be equal to 0.05mm at the weld toe for thicknesses lower than 5mm. A notch radius equal to 0.05mm is always recommended for crack-like notches (e.g. at the weld root). To achieve convergence of the local stress field, the local element size should be approximately one-tenth of the notch radius.

Ansys Mechanical FE software was used to generate the three input models of the welded K-node, as shown in Fig. 3, in accordance with the modelling guidelines for the FEMFAT software. More specifically:

(i) An FE *shell* model of the welded K-node was developed by modelling the intermediate surfaces of the chord and brace tubes. Half of the joint was modelled using the XY symmetry plane (see Fig. 1a). The geometry of the weld beads was not included. Table 2 shows that a free 8-node FE *shell* mesh (SHELL 281 from the Ansys FE library) was generated, with an element size of $2t = 40mm$ overall. Here, t represents the minimum sheet metal thickness in the model (i.e. the thickness of the braces elements). Loads and constraints were applied as shown in Fig. 3a to replicate the loading conditions in the experimental fatigue tests. The time required to solve the linear elastic FE analysis in Ansys Mechanical was four seconds (see Table 2). The resultant Ansys CDB file (approximately 2.7MB), containing the finite element mesh data (i.e. nodes and elements), and the RST file (approximately 7.2MB), containing the stress amplitude results, were extracted for import into FEMFAT.

(ii) A *solid* volume-based FE model of the welded K-node was developed by modelling only half of the geometry, since it is symmetrical with respect to the XY plane (see Fig. 3b). The model included detailed, realistic, full-penetration weld geometry, with the brace and chord-side weld toes modelled as sharp, V-shaped notches. In accordance with the FEMFAT *Solid*WELD meshing guidelines, a free mesh comprising 10-node tetrahedral finite elements (SOLID 187 from the Ansys FE library) was generated with a local element size of 1mm around the weld toes. The size was specified in the weld bead region and extended approximately 20mm from the weld toe lines. Outside the locally refined mesh region, the size of the tetrahedral elements was gradually increased to 20mm (equivalent to the brace thickness, t) in order to decrease the mesh density as much as possible and generate only one element in the thickness of the brace tube. Finally, all the *Solid*WELD nodes (i.e. the nodes located at the weld toes) were collected into a named selection called *"FemfatSolidWeld_1_toe_y-joint_30p0"*, in accordance with the FEMFAT *Solid*WELD naming guidelines. Here, *"toe"* specifies the type of weld edge, and *"30p0"* refers to the maximum thickness between the welded members of the K-node (i.e. the chord tube thickness). Solving the linear elastic FE analysis in Ansys Mechanical took approximately 11

FE model	Adopted finite element type (code in Ansys FE library)	Global FE size [mm]	Local FE size [mm]	Number of DOF*	FEA solution time [s] ^
Figure 3a	8-node shell (SHELL 281)	40	40.0	$8.30 \cdot 10^4$	4
Figure 3b	10-node tetrahedral (SOLID 187)	20	1.0	$1.75 \cdot 10^7$	644 ~ 11 minutes
Figure 3c	10-node tetrahedral (SOLID 187)	20	0.1	$1.02 \cdot 10^8$	$1.2 \cdot 10^4$ ~ 3.33 hours

^ Machine hardware: CPU: Intel Core i9-10900X @ 3.70GHz; RAM: 128GB; GPU: NVIDIA T400, 4GB.
** For 10-node tetrahedral elements, there are three degrees of freedom per node; for 8-node shell elements, there are five degrees of freedom per node.*

Table 2. Finite element types and sizes used to generate input FE models in Ansys Mechanical software.

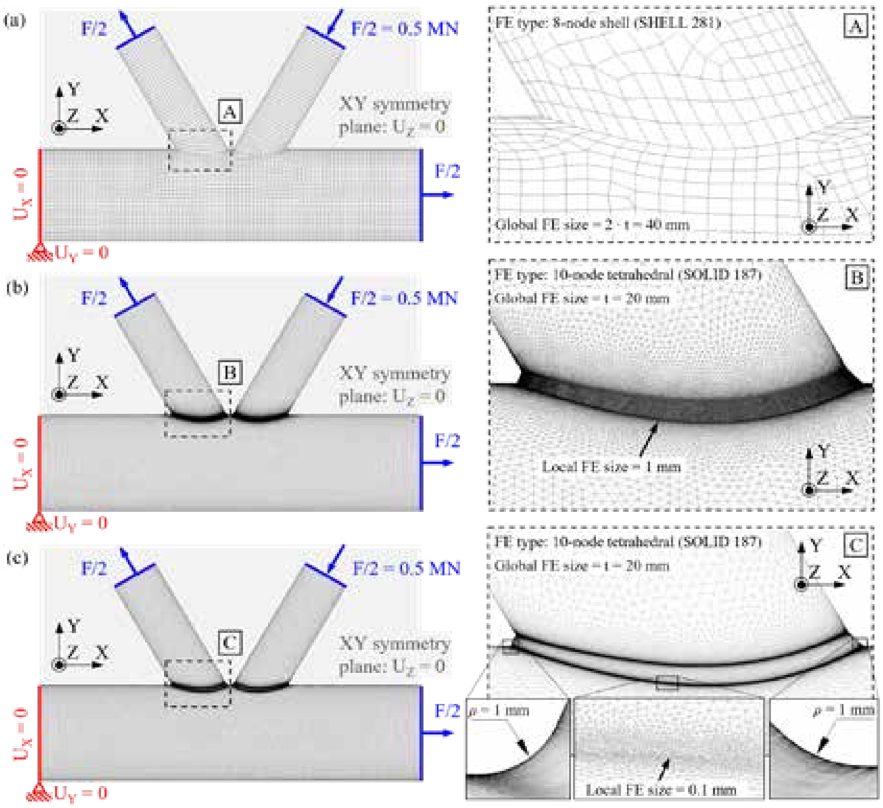

Fig. 3. The K-node FE models generated in Ansys Mechanical and adopted for fatigue strength analysis using MAGNA FEMFAT software. (a) A detail of the 8-node shell FE model using the FEMFAT Shell WELD approach. (b) A detail of the 10-node tetrahedral solid FE model with modelled weld beads using the FEMFAT SolidWELD approach. (c) A detail of the 10-node tetrahedral solid FE model with modelled weld beads and a $\rho = 1mm$ notch radius at the weld toes using the R1MS approach.

minutes (see Table 2). The resulting Ansys CDB file (approximately 1.4GB), which contains the FE mesh data (i.e. nodes and elements), and the RST file (approximately 3GB), which contains the stress amplitude results, were extracted for import into FEMFAT.

(iii) A *solid* volume-based FE model of the welded K-node was developed by modelling only half of the geometry, as it is symmetric with respect to the XY plane (see Fig. 3c). As in the previous case (ii), the model included the detailed geometry of the full-penetration weld beads. Additionally, a $\rho = 1mm$ notch radius was introduced at the weld toes for both the brace and the chord members. Free meshing with 10-node, tetrahedral SOLID 187 fine elements (from the Ansys FE library) was generated. A local dimension of 0.1mm (i.e. $\rho/10$) was assigned to the notch faces extending to the weld toe (see Fig. 3c). Then, the free meshing algorithm in Ansys Mechanical was used to progressively increase the size of the finite elements away from the notch regions. To ensure the presence of at least one element through the thickness of the brace member, t, a 20mm element size was chosen. According to the FEMFAT R1MS naming guidelines, all FE nodes along the weld toes were collected in a *named selection* called *"C200"*. Solving the linear elastic FE analysis in Ansys Mechanical took approximately 3.33 hours (see Table 2). The resulting Ansys CDB file containing the FE mesh data (i.e. nodes and elements) was approximately 8.2GB. The RST file, which contains the stress amplitude results, was approximately 15GB. Both files were extracted and imported into FEMFAT for the fatigue strength analysis.

The input models (i)–(iii) were defined in Ansys Mechanical, exported as CDB files containing the FE mesh entities (i.e. nodes and elements), and imported into the FEMFAT fatigue analysis tool.

For the *shell* input model of the FEMFAT *Shell* WELD analysis (see Fig. 3a), the automated routine in the FEMFAT *Visualizer* that identifies seam lines between the chord and braces tubes (i.e. the weld edges) was used successfully. Two reference joint categories were identified in the available FEMFAT structural steel joint detail databases: (1) the "T90-JOINT (FAT80/100)" weld detail from the *Eurocode 3/9* database (Fig. 4a), and (2) the "TJOINT – HV Seam" weld detail from the *ECS standard* database (Fig. 4b). Both details pertain to a one-sided, full-penetration weld in a T-joint with a 90-degree inclination angle between the main and stiffener plates (see Fig. 4). This represents the welded connection between the chord and braces locally. Finally, the same joint detail was assigned to each node along the identified *weld edges.*

No pre-processing operations were required to define the welded connection between the chord and the braces in the input solid model used for the FEMFAT *Solid*WELD analysis (see Fig. 3b). This is because the model already displays the detailed weld bead geometry and the nodes along the brace-side and chord-side weld toes are automatically detected by FEMFAT during geometry import. These nodes were collected in the *"FemfatSolidWeld_1_toe_y-joint_30p0" named selection*. Similarly, in the case of the *solid* model for the FEMFAT R1MS analysis (see Fig. 3c), the weld nodes belonging to the 1mm-notch faces were automatically detected and collected by FEMFAT in the *"C200" named selection.* This eliminated the need for additional manual pre-processing activities.

All FEMFAT analyses have been performed using the FEMFAT *ChannelMAX* module. This enables the FE analyst to:

- import the stress amplitude results extracted from the Ansys Mechanical FE software and assign them to one or more *Channels* based on the number of load steps stored in the FE results file;
- import or define a time-history of applied stresses in terms of normalized stress amplitude (e.g. σ/σ_{max}); and
- specify a multiplication factor for the imported stresses, if required.

FEMFAT Approach	WELD Database WELD Detail	WELD Method	Miner Formulation	Number of Analysed Nodes	FEMFAT Solution Time ^	
					CA*	VA**
Shell WELD	Eurocode 3/9 database T90JOINT - FAT80/100	*Eurocode 3/9*	Eurocode 3/9 (= Miner Modified)	86	2 seconds	3 minutes
Shell WELD	ECS database TJOINT - HV Seam	*FEMFAT 4.7*	Miner Modified	86	2 seconds	3 minutes
SolidWELD	-	*FEMFAT 4.7*	Miner Modified	7,016	60 seconds	60 minutes
R1MS	-	*FEMFAT 4.7*	Miner Elementary	803,344	15 minutes	20 hours

^ Adopted hardware: CPU: Intel Core i9-10900X @ 3.70GHz; RAM: 128GB; GPU: NVIDIA T400, 4 GB.
** Solution time required for one FEMFAT analysis of Constant Amplitude (CA) loads.*
*** Solution time required for one FEMFAT analysis of Variable Amplitude (VA) loads.*

Table 3. Summary of fatigue strength analyses performed using FEMFAT software.

In Ansys Mechanical, it is worth noting that the three forces acting on the braces and chord of the K-node (see Fig. 1) were applied in a single load step. Therefore, a single *Channel* and load time-history of the applied stress amplitudes, taking the total applied load into account, is sufficient (see Fig. 3).

The following procedures were adopted for of the models shows in Fig. 3:

- For constant amplitude (CA) fatigue loads, the Ansys RST results file was imported using a single FEMFAT *Channel*. A single load cycle acting on the K-node was simulated by defining a fully reversed normalized *triangular* load history (R=-1) using the Time Histories in FEMFAT.

For variable amplitude (VA) fatigue loads, the Ansys RST results file was imported using a single FEMFAT *Channel*. The COLOS stress spectrum was then converted into a load history with a load ratio of R=-1 a spectrum length of $L_s=4.94 \cdot 10^5$ cycles (1 point/cycle) and $p=0.15$ (see Fig. 2). This was done in accordance with the experimental testing framework. An RPC file of the time-history was then generated and imported in accordance with the FEMFAT guidelines.

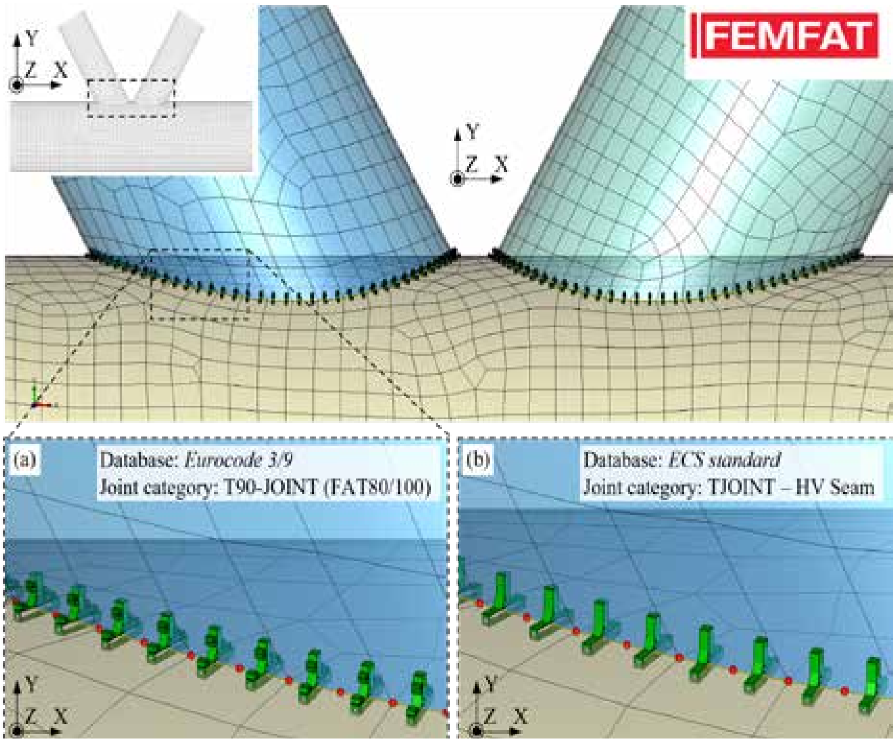

Fig. 4. Definitions of weld edges and the associated joint categories in FEMFAT Visualizer, as defined in (a) the Eurocode 3/9 database and (b) the ECS database.

The *material generator* in FEMFAT was used to quickly define all the necessary material data, which is specified as follows:

- Ultimate strength: 515MPa;
- Yield strength: 362MPa;
- Young's modulus: 206000N/mm^2; and
- Elastic poisson's Ratio: 0.28

This is in accordance with the data reported by the original author [1].

The material properties were applied to all the model nodes in the *Node Characteristics* section. For the FEMFAT R1MS analysis, the *"WELD-ASTM-50_toe_r=1_mm_ECS.ffd"* material database was imported in accordance with the FEMFAT R1MS guidelines. The relevant material properties were then applied to the nodes in the *"C200"* group in the *Node Characteristics* section.

A total of 32 FEMFAT analyses were conducted based on the experimental data presented in Table 1 using four types of FEMFAT fatigue strength analysis. Table 3 shows the main parameters adopted for each analysis, alongside the corresponding solution time. More specifically, there were:

(a) Eight fatigue analyses were performed using the FEMFAT *Shell* WELD approach in conjunction with the *Eurocode 3/9* analysis method (see Table 3). The *shell* FE model in Fig. 3a was used as input. The WELD setting, which uses the *Eurocode 3/9* method, was enabled in FEMFAT. The *"Signed Mises (Sign from Sigma_perpendicular)"* equivalent stress was selected to use the available von Mises-based formulation and combine the notch stress amplitude components into an equivalent notch stress amplitude at each analysed *weld node* according to the following expression [4]:

$$\sigma_{eq,VM} = sign(\sigma_{a\perp})\sqrt{\sigma_{a\perp}{}^2 + \sigma_{a\parallel}{}^2 + \sigma_{a\perp}\cdot\sigma_{a\parallel} + 3\cdot\tau_a{}^2}$$

Equation (1)

Where:

- $\sigma_{a\perp}$ is the amplitude of the normal stress at the notch that acts orthogonally to the *weld edge;*
- $\sigma_{a\parallel}$ is the amplitude of the normal stress at the notch that runs parallel to the *weld edge;*
- τ_a is the amplitude of the tangential stress at the notch.

For a complete overview of the theoretical background, please refer to the FEMFAT guidelines [4].

The *Automatic Stress Correction* function in the WELD Stress settings was enabled, and the *Stress Interpolation* Parameters $A = B = 0.280$ and $C = 0.000$ were adopted. This ensured that the local stresses were extracted 14mm from the junction line between the chord shell plate and the brace *shell* plate. This corresponds to the approximate position of the *weld* toe of the chord tube.

Finally, the *Statistical General Factor* was used to set a 50% probability of survival, which was adopted for fatigue strength estimates. No other *Influence Factors* were considered in the analysis. The *Analysis Target* was set to *Damage*, and the Miner formulation of *Eurocode 3/9* was specified for the damage calculation. The default cutoff limit of 10^8 cycles was maintained for the S-N curve.

As stated in the FEMFAT guidelines, it is important to note that the *Eurocode 3/9* formulation aligns with the *Miner Modified* formulation. A 50% probability of survival was specified in the *Global Parameters*. No additional *Analysis Parameters* were required. A fatigue strength assessment was conducted on the *86 weld nodes* (i.e. the nodes along the identified *weld edges*) as reported in Table 3. This table was previously compiled in a dedicated group in FEMFAT. Each *Shell* WELD analysis using the *Eurocode 3/9* method took two seconds to solve for the CA loads and three minutes for the VA loads.

(b) A total of eight fatigue analyses were performed using the FEMFAT *Shell* WELD approach combined with the *FEMFAT 4.7* method (see Table 3). As in case (a) above, the FE *shell* model in Fig. 3a was used as input. The WELD setting was enabled using the *FEMFAT 4.7* analysis method. The WELD settings previously described in (a) were adopted here as well. The *Statistical General Factor* was enabled to account for a 50% probability of survival in fatigue strength calculations. The *Analysis Target* was set to *Damage*, and the *Miner Modified* formulation was specified for the damage calculation. A *probability of survival* was specified in the *Global Parameters.* Finally, the *Absolute Stress Limit* for the WELD in the *Analysis Filter* was set to 0N/mm^2.

This allowed FEMFAT to consider all stress amplitudes during the damage analysis rather than filtering out the low ones. It is important to note that FEMFAT did not use this *filter analysis parameter* in the *Eurocode 3/9* method (see point (a) above). The fatigue strength evaluation was conducted on 86 *weld nodes* that were previously collected in a dedicated FEMFAT *group* (see Table 3). Each *Shell* WELD analysis combined with the *FEMFAT 4.7* method took two seconds for the CA load cases and three minutes for the VA load cases.

(c) A total of eight fatigue analyses were performed using the FEMFAT *Solid*WELD approach in conjunction with *FEMFAT 4.7* method for post-processing the linear elastic stresses (see Table 3). The solid FE model shown in Fig. 3b was used as input data. The WELD setting was enabled in FEMFAT using the *FEMFAT 4.7* analysis method. Equivalent stress *("Signed Mises-Stress 1, sign from maximum principal stress)* was selected to analyse the *Solid*WELD nodes. The von Mises-based formulation was used to combine the notch stress amplitude components at each analysed node according to Eq. (1). For a complete overview of the theoretical background and other available formulations for equivalent peak stress at *Solid*WELD nodes, please refer to the FEMFAT guidelines.

The *Statistical General Factor* was used to set a 50% probability of survival, and this was taken into account in the fatigue strength calculations. No other *Influence Factors* were considered in the analysis. The *Analysis Target* was set to *Damage* and the *Miner Modified* formulation was specified for the damage calculation. The von Mises equivalent stress method and a 50% probability of survival were assigned in the *Global Parameters*.

As *Solid*WELD nodes are part of the base material, the *Absolute Stress Limit for Base Material* in the Analysis Filter was set to 0N/mm^2 to deactivate the low stress amplitude filter during damage analysis. A fatigue strength assessment was conducted on 1,056 *Solid*WELD nodes (i.e. nodes located at the brace and chord weld toes), as shown in Table 3. These nodes were previously isolated in the *"FemfatSolidWeld 1toe y-joint 30p0"* named selection in Ansys Mechanical and then imported into FEMFAT. Each *Solid*WELD analysis combined with the *FEMFAT 4.7* method required 60 seconds of solution time for the CA load cases and 60 minutes for the VA load cases.

(d) A total of eight fatigue analyses were performed using both the FEMFAT R1MS approach and the *FEMFAT 4.7* method (see Table 3). The *solid* FE model shown in Fig. 3c was used as input data. The WELD setting was enabled in the settings for the *FEMFAT 4.7* analysis method. As in previous cases (a)–(c), the *Statistical General Factor* was included to relate the fatigue strength estimates to 50% probability of survival. No additional *Influence Factors* were considered in the analysis. In line with previous analyses (a)–(c), the *Analysis Target* was set to *Damage* and the *Miner Elementary* formulation was specified for the damage calculation. This ensures that the slope of the S-N curve adopted in calculations extends beyond the cut-off limit (see Fig. 11).

The von Mises equivalent stress method and a *50% probability of survival* was specified as the *Global Parameters*. Since FEMFAT considers the target nodes belonging to the notch faces to be part of the base material, the *Absolute Stress Limit* for Base Material in the *Analysis Filter* was set to $0N/mm^2$ to prevent filtering at low stress amplitudes during the damage analysis.

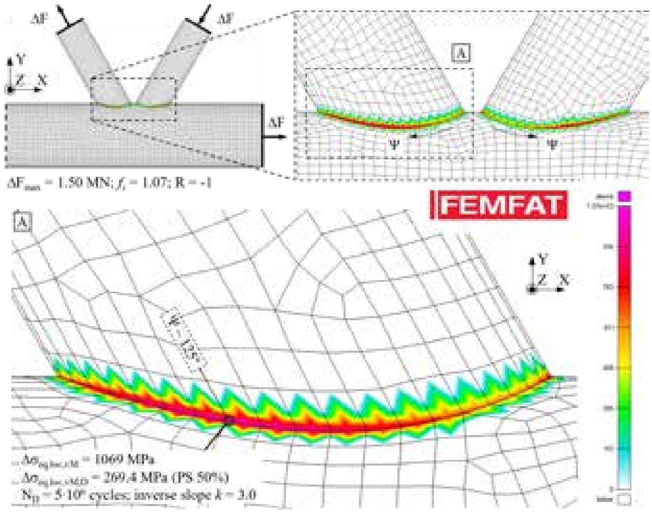

Fig. 5. The Von Mises equivalent stress range for specimen "6, CA" (see Table 1) using the FEMFAT Shell WELD approach in conjunction with the Eurocode 3/9 WELD method.

Fatigue strength evaluations were conducted on 803,344 nodes belonging to the 1mm notch faces (see Table 3). These nodes were initially collected in the *"C200" named selection* within Ansys Mechanical and then imported into FEMFAT. Each R1MS analysis combined with the *FEMFAT 4.7* method took 15 minutes to solve for the CA load cases and approximately 20 hours for VA load cases.

Figs. 5–8 show the results of FEMFAT analyses (a)–(d), calculated in terms of equivalent von Mises stress range ($\Delta\sigma_{eq,loc,vM}$) at the FE nodes analysed. They are represented graphically on a mesh view of the model via *contour plots* generated by the FEMFAT *Visualizer* tool. This example relates to the "6, CA" welded specimen in Table 1.

Fig. 5 shows the *contour plot* of the von Mises equivalent stress range, which was calculated along the *weld edges* and analysed using the FEMFAT *Shell* WELD approach in combination with the *Eurocode 3/9* method. The most critical point is located at $\Psi \sim 125°$ on the *weld edge* between the chord tube and brace tube 1. Furthermore, von Mises equivalent stress range values comparable to the maximum value within a 5% deviation are obtained along the *weld edge* of brace tubes 1 and 2, in regions extending approximately from $\Psi = 90°$ to $\Psi = 140°$ and $\Psi = 90°$ to $\Psi = 120°$, respectively. There is good agreement between the resulting critical points (Fig. 5) and the crack initiation sites observed during the experimental tests. According to references [1–3] (see Table 1), these sites range between $\Psi = 90°$ and $\Psi = 135°$.

Fig. 6 shows the *contour plot* of the von Mises equivalent stress *amplitude* calculated along the *weld edges* using a combination of the FEMFAT *Shell* WELD approach and *FEMFAT 4.7* analysis method. The most critical point is located at $\Psi \sim 125°$ on the weld edge of brace tube 1. This is consistent with the result obtained using the *Eurocode 3/9* method (see Fig. 5). In addition, von Mises equivalent stress amplitude values comparable to the maximum value within a 5% deviation are obtained along the *weld edge* of brace tube 1 in a region extending approximately between $\Psi = 100°$ and $\Psi = 150°$, as well as along the *weld edge* of brace tube 2 in a region extending between $\Psi = 100°$ and $\Psi = 120°$. As in Fig. 5, there is a good agreement between the resultant critical points (Fig. 6) and the experimental crack initiation sites, which range between $\Psi = 90°$ and $\Psi = 135°$ [1–3] (see Table 1).

Fig. 7 shows the *contour plot* of the von Mises equivalent stress *amplitude*, as calculated using the FEMFAT *Solid*WELD approach and the *FEMFAT 4.7* analysis method at the brace- and chord-side weld toes. The node with the maximum von Mises equivalent stress *amplitude* value (i.e. the most critical point) is located at $\Psi \sim 110°$ along the chord-side weld toe, between the chord tube and brace tube 1. Comparable von Mises equivalent stress amplitude values within a 5% deviation from the maximum value are obtained along the chord-side weld toe of brace tube 1, extending from approximately $\Psi = 90°$ to $\Psi = 135°$, as well as

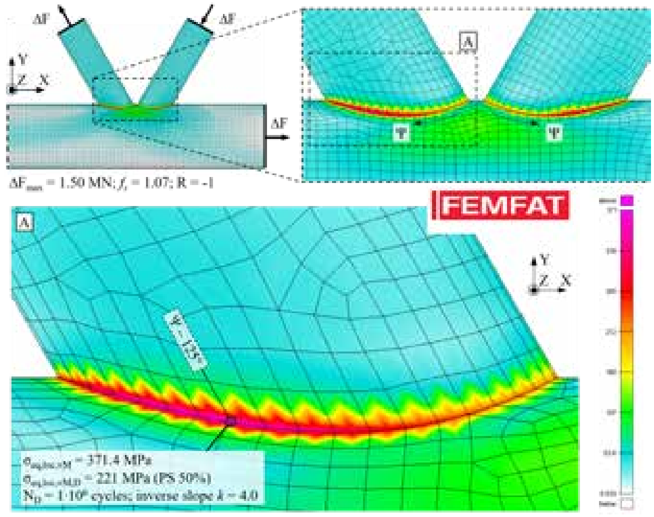

Fig. 6. The Von Mises equivalent stress amplitude for specimen "6, CA" (see Table 1) using the FEMFAT Shell WELD approach combined with the FEMFAT 4.7 WELD method.

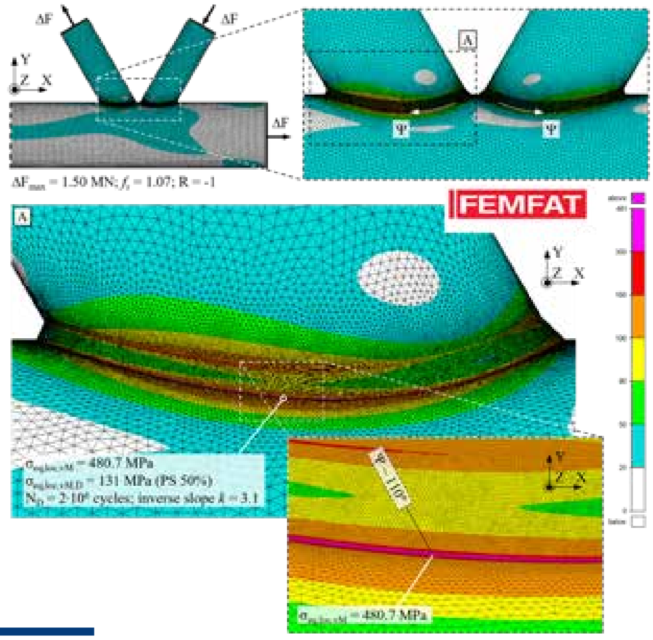

Fig. 7. The Von Mises equivalent stress amplitude results for specimen "6, CA" using the FEMFAT SolidWELD approach in conjunction with the FEMFAT 4.7 WELD method.

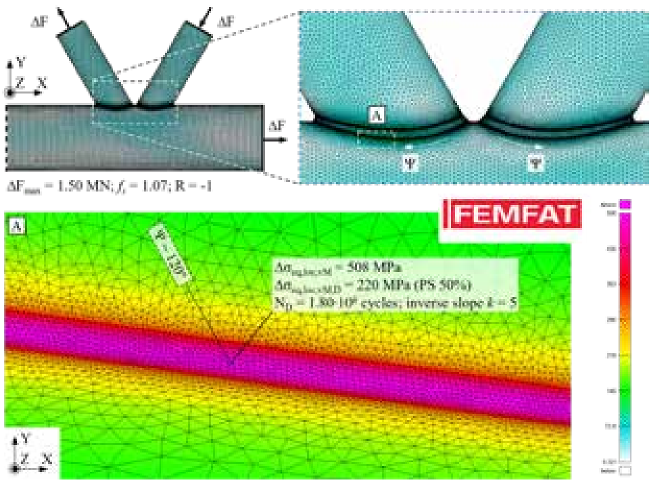

Fig. 8. The Von Mises equivalent stress range for specimen "6, CA" (see Table 1) using a combination of the FEMFAT R1MS approach and the FEMFAT 4.7 WELD method.

along the chord-side weld toe of brace tube 2 in a region extending from approximately $\Psi = 90°$ to $\Psi = 120°$. There is very good agreement between the estimated critical points (Fig. 7) and the experimental crack initiation sites, which range between $\Psi = 90°$ and $\Psi = 135°$ [1–3] (see Table 1).

Finally, Fig. 8 shows the von Mises equivalent stress *range contour plot*, which was calculated using the FEMFAT R1MS and approach and *FEMFAT 4.7* analysis method. The analysis was performed at the brace-side and chord-side weld toes. The area in which the maximum von Mises equivalent stress range value is obtained is the most critical point. This point is located at $\Psi \sim 120°$ on the chord-side weld toe, between the chord tube and brace tube 1. Similar von Mises equivalent stress *range* values, deviating by no more than 5% from the maximum value, are at the chord-side weld toe of brace tube 1, within a region extending from approximately $\Psi = 70°$ to $\Psi = 150°$. The same is true for the chord-side weld toe of brace tube 2, within a region extending from approximately $\Psi = 100°$ to $\Psi = 150°$. Once again, there is excellent agreement between the estimated critical points (Fig. 8) and the experimental crack initiation sites, which vary between $\Psi = 90°$ and $\Psi = 135°$ [1–3] (see Table 1).

Comparison of experimental fatigue results and fatigue lifetime estimations

The experimental fatigue results presented in Table 1, originally in terms of the applied load range (ΔF), were re-evaluated in terms of the equivalent von Mises stress range. This was achieved using the following approaches:

- the FEMFAT *Shell* WELD approach combined with *Eurocode 3/9* analysis method (see Fig. 5).
- the FEMFAT *Shell* WELD approach combined with *ECS standard* analysis method (see Fig. 6).
- the FEMFAT *Solid*WELD approach combined with *ECS standard* analysis method (see Fig. 7).
- the FEMFAT R1MS approach combined with the *ECS standard* analysis method (see Fig. 8).

A dedicated *stress amplitude* scale factor was calculated for each data point in Table 1. For each FE model analysed, the stress amplitude data imported from Ansys was multiplied by the relevant *stress amplitude scale factor* to account for the actual load amplitude applied in the experimental tests and the effect of corrosion in sea-water.

$$f_s = \frac{1}{f_c} \cdot \frac{\Delta F_{exp.max}}{2 \cdot F_{FEA}} \qquad \textit{Equation (2)}$$

In the above expression:

- $\Delta F_{exp.max}$ represents the maximum load range applied in the experimental fatigue test.
- F_{FEA} is the amplitude of the load applied in the FE analysis performed in Ansys Mechanical (*i.e.* $F = 1\ MN$; see Fig. 3).
- $f_c = 0.7$ considers the impact of corrosion, as outlined in GL 2007 [5].

It is worth noting that sea-water corrosion generally reduces the fatigue strength of welded joints. Consequently, the fatigue limit of the S-N design curve used for the fatigue strength assessment must be multiplied by the f_c factor, as described in reference [5]. This ultimately reduces the fatigue strength by 30%. However, the FEMFAT software does not currently incorporate an *Influence Factor* to account for corrosion's effect on the fatigue limit of the presented S-N curves. To address this issue, the f_c factor was incorporated into the stress *amplitude scale factor* (f_s). This allows the experimental fatigue data to be corrected prior to fatigue analysis, without modifying the S-N curves employed by FEMFAT in its calculations.

Figs. 9–12 show a comparison of the re-evaluated experimental data with the S-N design curves for steel welded joints as adopted by FEMFAT for each of the four analysis approaches considered (see Table 4). The reported markers relate to the experimental data in terms of

- the number of cycles to crack initiation (N_{init})
- the number of cycles to breakthrough (i.e. when a through-the-thickness crack occurs at the weld toe on the chord side (N_{bt})).

For each approach in Table 4 and each specimen in Table 1, the number of cycles predicted by FEMFAT can be determined by horizontally intersecting the relevant S-N design curve (PS 50% or PS 97.7%) with the given $\Delta\sigma_{eq,vM}$ value, as shown in Figs. 9–12. Accordingly, results to the left of the PS 50% S-N design curve indicate that crack initiation occurred in the experiments, before the estimated fatigue failure. These results are therefore considered unsafe.

FEMFAT approach	FEMFAT WELD method	Slope k	Slope k'	$\Delta\sigma_D$ (PS50%) [MPa]	N_D [cycles]
Shell **WELD**	*(a) Eurocode 3/9*	3.0	5.0	269.4	$5.00 \cdot 10^6$
Shell **WELD**	*(b) FEMFAT 4.7*	4.0	7.0	442	$1.00 \cdot 10^6$
Solid**WELD**	*(c) FEMFAT 4.7*	3.1	5.2	262	$2.00 \cdot 10^6$
R1MS	*(d) FEMFAT 4.7*	5.0	5.0	220	$1.80 \cdot 10^6$

Table 4. Summary of the S-N fatigue design curves implemented by FEMFAT (also see Figs. 9–12).

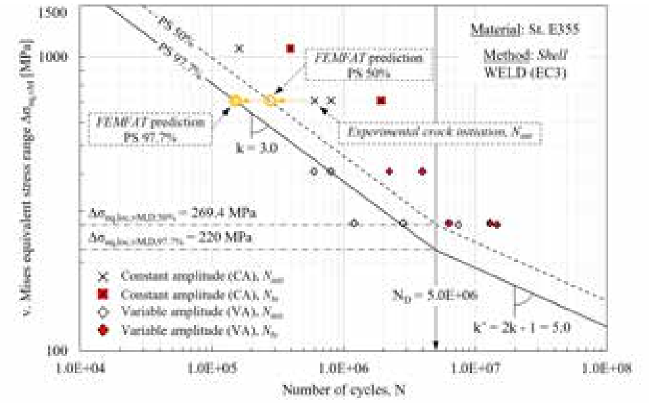

Fig. 9. Fatigue strength assessment of welded K-nodes using the FEMFAT Shell WELD approach in conjunction with the Eurocode 3 analysis method. The fatigue design curve for welded steel joints, as defined by Eurocode 3 and recorded in the FEMFAT database, was compared with experimental fatigue data obtained from constant and variable amplitude fatigue tests (see references [1–3]).

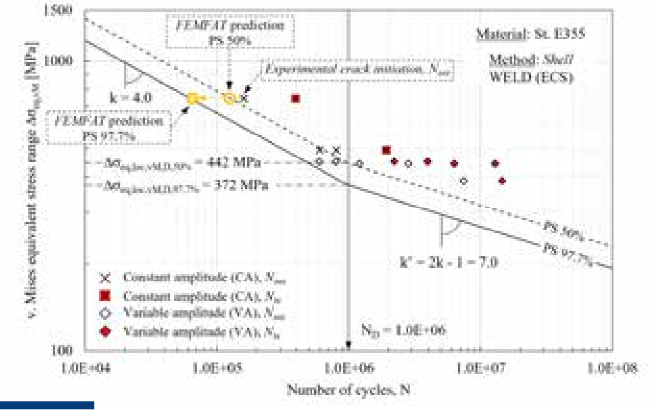

Fig. 10. Fatigue strength assessment of welded K-nodes using the FEMFAT Shell WELD approach in combination with the FEMFAT 4.7 analysis method. The fatigue design curve for welded steel joints, as defined by the ECS standard in the FEMFAT database, was compared with the experimental fatigue data from constant and variable amplitude fatigue tests referenced in [1–3].

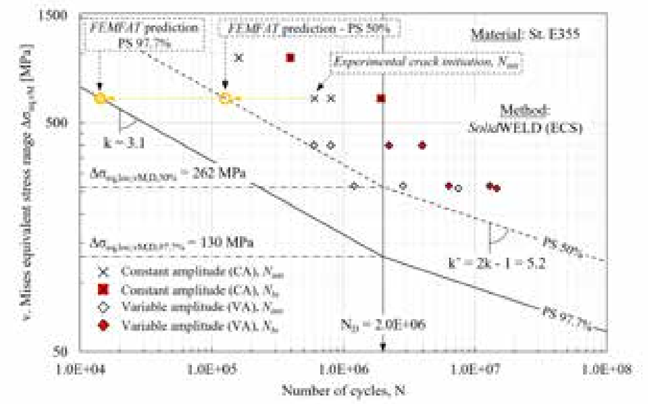

Fig. 11. Fatigue strength assessment of welded K-nodes using the FEMFAT SolidWELD approach and the FEMFAT 4.7 analysis method. It compares the fatigue design curve for welded steel joints as defined by the ECS standard in the FEMFAT database and with experimental fatigue data from constant and variable amplitude fatigue tests referenced in [1–3].

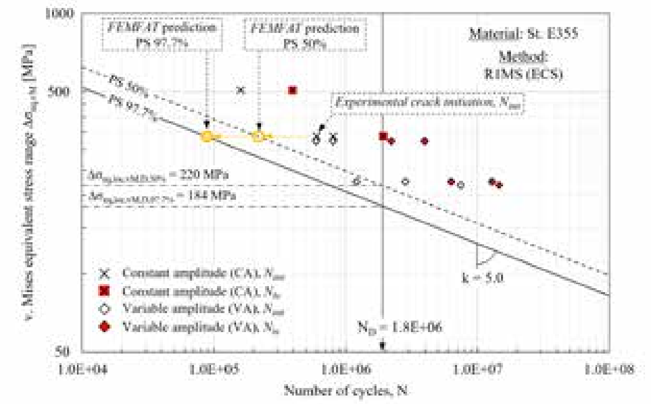

Fig. 12. Fatigue strength assessment of welded K-nodes using the FEMFAT R1MS approach together with the FEMFAT 4.7 analysis method. The fatigue design curve for welded steel joints, as defined by the ECS standard in the FEMFAT database, is compared with the experimental fatigue data from constant and variable amplitude fatigue tests referenced in [1–3].

Conversely, results to the right of the PS 50% S-N design curve are considered safe, indicating that the actual crack initiation during the experiment occurred after the estimated fatigue lifetime. Finally, Table 5 summarizes the comparison between the experimental results and FEMFAT's predictions in terms of the number of cycles to crack initiation at 50% and 97.7% probability of survival.

Fig. 9 shows a comparison of the fatigue design curve for steel welded joints as defined by Eurocode 3, with experimental fatigue data obtained from constant and variable amplitude fatigue tests referenced in [1–3]. This data was then re-evaluated in terms of the von Mises equivalent stress range calculated at the most critical point using the FEMFAT *Shell* WELD approach in conjunction with the *Eurocode 3/9* analysis method (see Fig. 5).

The S-N curve is defined by a slope $k = 3$ and a fatigue limit of $\Delta\sigma_D = 269.4MPa$ (PS 50%) at $N_D = 5{\cdot}10^6$ cycles. According to the *Miner Modified* formulation (see Table 3), a slope of $k' = 2k\text{-}1 = 5$ is adopted for $N > N_D$ (see Table 4). Table 5 compares the number of cycles to crack initiation in the experiments with the estimated fatigue life using the aforementioned FEMFAT S-N design curve and 50% probability of survival for each specimen. In the case of CA loads and a 50% probability of survival, all three of the experimental results relating to crack initiation are considered safe. Conversely, with VA loads and a 50% probability of survival, only one of the five crack initiation experiment results is deemed safe. Ultimately, all CA and VA results relevant to the break-through lie within the safe zone of the S-N design curve.

Fig. 10 shows a comparison of the fatigue design curve for steel welded joints, as defined by the ECS standard in the FEMFAT database, and re-evaluated experimental fatigue data from constant and variable amplitude fatigue tests from [1–3] in terms of the von Mises equivalent stress range. The von Mises equivalent stress range was calculated at the most critical point using the FEMFAT *Shell* WELD approach in conjunction with the *FEMFAT 4.7* analysis method (see Fig. 6).

The local S-N curve at the most critical node is defined by a slope $k = 4$ and a fatigue strength limit of $\Delta\sigma_D = 442MPa$ (PS 50%) at $N_D = 1{\cdot}10^6$ cycles. According to the *Miner Modified* formulation (see Table 3), a slope $k' = 2k\text{-}1 = 7$ is adopted for $N > N_D$ (see Table 4). Table 5 shows a comparison of the number of cycles to crack initiation in experiments with the estimated fatigue life using the proposed FEMFAT S-N design curve, given a 50% probability of survival.

Specimen No.	Crack initiation Experimental results	FEMFAT prediction Shell WELD (EC3) Fig. 9		FEMFAT prediction Shell WELD (ECS) Fig. 10		FEMFAT prediction *Solid*WELD (ECS) Fig. 11		FEMFAT prediction R1MS (ECS) Fig. 12	
		$N_{predicted}$ [cycles]		$N_{predicted}$ [cycles]		$N_{predicted}$ [cycles]		$N_{predicted}$ [cycles]	
	N_{init} [cycles]	PS 50%	PS 97.7%	PS 50%	PS 97.7%	PS 50%	PS 97.7%	PS 50%	PS 97.7%
6, CA	$1.60 \cdot 10^5$	$8.00 \cdot 10^4$	$4.36 \cdot 10^4$	$1.25 \cdot 10^5$	$6.29 \cdot 10^4$	$3.55 \cdot 10^4$	$4.05 \cdot 10^3$	$2.75 \cdot 10^4$	$1.13 \cdot 10^4$
7a, CA	$6.00 \cdot 10^5$	$2.74 \cdot 10^5$	$1.49 \cdot 10^5$	$6.47 \cdot 10^5$	$3.25 \cdot 10^5$	$1.27 \cdot 10^5$	$1.44 \cdot 10^4$	$2.14 \cdot 10^5$	$8.76 \cdot 10^4$
7b, CA	$8.05 \cdot 10^5$	$2.74 \cdot 10^5$	$1.49 \cdot 10^5$	$6.47 \cdot 10^5$	$3.25 \cdot 10^5$	$1.27 \cdot 10^5$	$1.44 \cdot 10^4$	$2.14 \cdot 10^5$	$8.76 \cdot 10^4$
1, VA	$5.93 \cdot 10^5$	$1.44 \cdot 10^6$	$7.83 \cdot 10^5$	$9.39 \cdot 10^5$	$4.71 \cdot 10^5$	$5.48 \cdot 10^5$	$6.24 \cdot 10^4$	$2.64 \cdot 10^5$	$1.08 \cdot 10^4$
10, VA	$8.00 \cdot 10^5$	$1.44 \cdot 10^6$	$7.83 \cdot 10^5$	$9.39 \cdot 10^5$	$4.71 \cdot 10^5$	$5.48 \cdot 10^5$	$6.24 \cdot 10^4$	$2.64 \cdot 10^5$	$1.08 \cdot 10^4$
13, VA	$7.42 \cdot 10^5$	$5.04 \cdot 10^6$	$2.75 \cdot 10^6$	$1.71 \cdot 10^6$	$8.57 \cdot 10^5$	$2.08 \cdot 10^6$	$2.37 \cdot 10^5$	$1.85 \cdot 10^6$	$7.59 \cdot 10^5$
3, VA	$2.82 \cdot 10^6$	$4.86 \cdot 10^6$	$2.65 \cdot 10^6$	$1.01 \cdot 10^6$	$5.05 \cdot 10^5$	$1.93 \cdot 10^6$	$2.19 \cdot 10^5$	$1.57 \cdot 10^6$	$6.42 \cdot 10^5$
2, VA	$1.20 \cdot 10^6$	$4.86 \cdot 10^6$	$2.65 \cdot 10^6$	$1.01 \cdot 10^6$	$5.05 \cdot 10^5$	$1.93 \cdot 10^6$	$2.19 \cdot 10^5$	$1.57 \cdot 10^6$	$6.42 \cdot 10^5$

Table 5. Overall comparison of the experimental results in terms of number of cycles to crack initiation with the numerical estimations using the S-N fatigue design curves implemented in FEMFAT (see Table 4).

For CA loads and a 50% probability of survival, two out of three experimental results relevant to crack initiation are considered safe, while one is considered unsafe. Conversely, for VA loads and a 50% probability of survival, three out of five experimental results relevant to crack initiation are considered safe, while two are considered unsafe. Overall, all CA and VA results relevant to the break-through lie on the safe side of the S-N design curve.

Fig. 11 shows a comparison of the fatigue design curves for steel welded joints as defined by the ECS standard in the FEMFAT database with experimental fatigue data obtained from constant and variable amplitude fatigue tests as reported in references [1–3]. This data was re-evaluated in terms of the von Mises equivalent stress range calculated at the most critical point, according to the FEMFAT *Solid*WELD approach combined with the *FEMFAT 4.7* analysis method (see Fig. 7).

The local S-N curve at the most critical node is defined by a slope $k = 3.1$ and endurance fatigue limit of $\Delta\sigma_D = 262MPa$ (PS 50%) at $N_D = 2{\cdot}10^6$ cycles. According to the *Miner Modified* formulation (see Table 3), a slope of $k' = 2k\text{-}1 = 5.2$ is adopted for $N > N_D$ (see Table 4). Table 5 compares the number of cycles to crack initiation in experiments with fatigue life estimates obtained using the previously described FEMFAT S-N design curve for a 50% probability of survival.

For CA loads and a 50% probability of survival, all three experimental crack initiation results fall within the safe range. For VA loads and a 50% probability of survival, four out of five crack initiation results in the experiments fall within the safe range, while one result lies within the unsafe range of the S-N curve (PS 50%). In the break-through conditions, all three CA results and all five VA results lie in the safe range of the S-N design curve.

Finally, Fig. 12 shows a comparison of the fatigue design curve for welded steel joints as defined by the ECS standard in the FEMFAT database, alongside experimental fatigue data obtained from constant and variable amplitude fatigue tests (see references [1–3]). This data was re-evaluated in terms of the von Mises equivalent stress range, calculated at the most critical point using the FEMFAT R1MS approach combined with the *FEMFAT 4.7* analysis method (see Fig. 8).

The local S-N curve at the most critical node is defined by a slope of $k = 5.0$ and a fatigue limit strength of $\Delta\sigma_D = 220MPa$ (PS 50%) at $N_D = 1.80{\cdot}10^6$ cycles. According to the Miner Elementary formulation (see Table 3), the same slope $k' = k = 5.0$ is used for $N > N_D$ (see Table 4). Table 5 compares the fatigue life predicted using the FEMFAT S-N design curve for the R1MS approach with the number of cycles to crack initiation observed in experiments on each specimen. For CA loads and a 50% probability of survival, all three experimental crack initiation results lie within the safe range. For VA loads and a 50% probability of survival, four out of five experimental results crack initiation results lie within the safe range, while one result lies outside this range. Ultimately, all CA and VA results relevant to the break-through are on the safe side of the S-N design curve.

Conclusions

The fatigue strength of large welded K-nodes in E355 structural steel was investigated numerically using the MAGNA FEMFAT commercial fatigue analysis software. According to the FEMFAT guidelines, four different fatigue strength assessment approaches were implemented in FEMFAT using three different FE model combinations created in Ansys Mechanical:

- the *Shell* WELD approach combined with the *Eurocode 3/9* analysis method,
- the *Shell* WELD approach combined with the *FEMFAT 4.7* analysis method,
- the *Solid*WELD approach combined with the *FEMFAT 4.7* analysis method, and
- the R1MS approach combined with the *FEMFAT 4.7* analysis method.

A set of experimental fatigue data relating to the geometry of the welded K-node under investigation, taken from the literature, was re-evaluated in terms of the von Mises equivalent stress range. These were then compared with the S-N fatigue design curves implemented by the FEMFAT software.

The automated analysis procedure implemented by FEMFAT enabled the fatigue strength of the welded connections between the brace and chord to be assessed using input FE models solved in Ansys Mechanical. Thanks to the meshing rules provided in the FEMFAT guidelines, a coarse global mesh was adopted for the shell input model. A locally refined mesh was required for the solid input model near the welds. However, a coarser mesh was used further away, significantly reducing the computational effort required for the FE analysis.

The FEMFAT tool enables users to:

- easily import FE mesh entities and relevant stress results for each input model.
- automatically identify *weld edges* in the case of the *shell* input model and assign suitable joint details for weld nodes based on the FEMFAT WELD databases.
- import a time-history of applied CA or VA loads;
- define the material properties;
- select the desired analysis method for assessing the fatigue strength of the welds according to *Eurocode 3/9* and *FEMFAT 4.7*.
- select the equivalent stress formulation to be used e.g. the von Mises equivalent stress; and
- select the damage calculation according to the Miner rule, e.g. *Miner Modified* and *Miner Elementary.*

All the approaches considered and described by FEMFAT successfully identified the most critical point of the welded connection between the brace tube and the chord tube in the saddle point region ($90° < \Psi < 125°$ in the least conservative case), in accordance with experimental fatigue crack evidence ($90° < \Psi < 135°$).

About the University of Padua's Department of Industrial Engineering (DII)

The Department of Industrial Engineering (DII) at the University of Padua is a centre of excellence for research and training in various engineering disciplines, including aerospace, chemical, electrical, energy, materials, and mechanical engineering. The department's mission is to promote innovation and competitiveness in industrial engineering through excellence in research and training.

Since its establishment in 2012 through the merger of six independent departments, the DII has grown to include 48 research laboratories and now offers four undergraduate (First Level) degrees, seven post-graduate (Second Level) degrees, two doctoral programs, and a variety of master's courses. The department employs over 500 people, including professors, researchers, doctoral students, and technical and administrative staff.

Around 50% of revenue is derived from collaborations with industries and research centres. The numerous spin-off companies demonstrate the DII's entrepreneurial spirit.

There was good agreement between the experimental crack initiation results and the proposed S-N curves when the FEMFAT *Shell* WELD approach was combined with the *Eurocode 3/9* and *FEMFAT 4.7* analysis methods.

The experimental data was distributed around the S-N design curve for a 50% probability of survival. For the FEMFAT *Solid*WELD approach, the experimental crack initiation data was mostly consistent with the PS 50% design curve. Besides the *Shell* WELD and the *Solid*WELD approaches, the R1MS approach was also used and provided safe estimates with respect to the experimental crack initiation data.

All of the fatigue strength assessment approaches considered provided safe fatigue durability estimates for the experimental data at break-through in relation to the PS 50% S-N curves. The FEMFAT fatigue analysis tool ultimately enabled the rapid evaluation of the large-scale K-node joint via the *Shell* WELD approach, thanks to the option of using a coarse mesh in the input FE model. Solving the FEMFAT *Shell* WELD analyses took less than five seconds for the CA loads and less than five minutes for the VA loads.

The *Solid*WELD approach required a longer solution time because a FE mesh with a 1mm refinement was needed at the weld toes. This equated to 60 seconds for CA loads and 60 minutes for VA loads. Ultimately, solving the R1MS analysis took up to 20 hours for VA loads, producing fatigue strength estimates comparable to those of the *Shell* WELD and *Solid*WELD approaches.

Using FEMFAT alongside the coarse mesh shell input models according to the *Shell* WELD method, significantly reduced the computational resources required to analyse the welded K-node, compared to the resources needed for the fatigue analysis using the complete *solid* model according to the *Solid*WELD approach.

For more information:

Professor Giovanni Meneghetti – University of Padova
giovanni.meneghetti@unipd.it

References

[1] D. Radaj, C. M. Sonsino, and W. Fricke, *Fatigue assessment of welded joints by local approaches,* Woodhead Publishing: Sawston, United Kingdom, 2006. HYPERLINK: doi.org/10.1533/9781845691882

[2] C. M. Sonsino, "Structural Durability Assessment of Welded Offshore K-Nodes by Different Local Design Concepts", *Frattura ed Integrità Strutturale*, vol. 3 (9), pp. 3–12, Jul. 2009, HYPERLINK: doi.org/10.3221/IGF-ESIS.09.01

[3] C. M. Sonsino, "Comparison of different local design concepts for the structural durability assessment of welded offshore K-nodes", *International Journal of Fatigue*, vol. 34, pp. 27–34, Jan. 2012, doi.org/10.1016/j.ijfatigue.2010.09.005

[4] *Magna Powertrain FEMFAT 2024 WELD User Manual*, MAGNA Powertrain, St. Valentin, Austria, 2024

[5] *GL Rules for Classification and Construction*, IV: Industrial Services, Part 6: Offshore Technology, Section 4: Structural Design, Germanischer Lloyd Aktiengesellschaft, Hamburg, Germany, 2007.

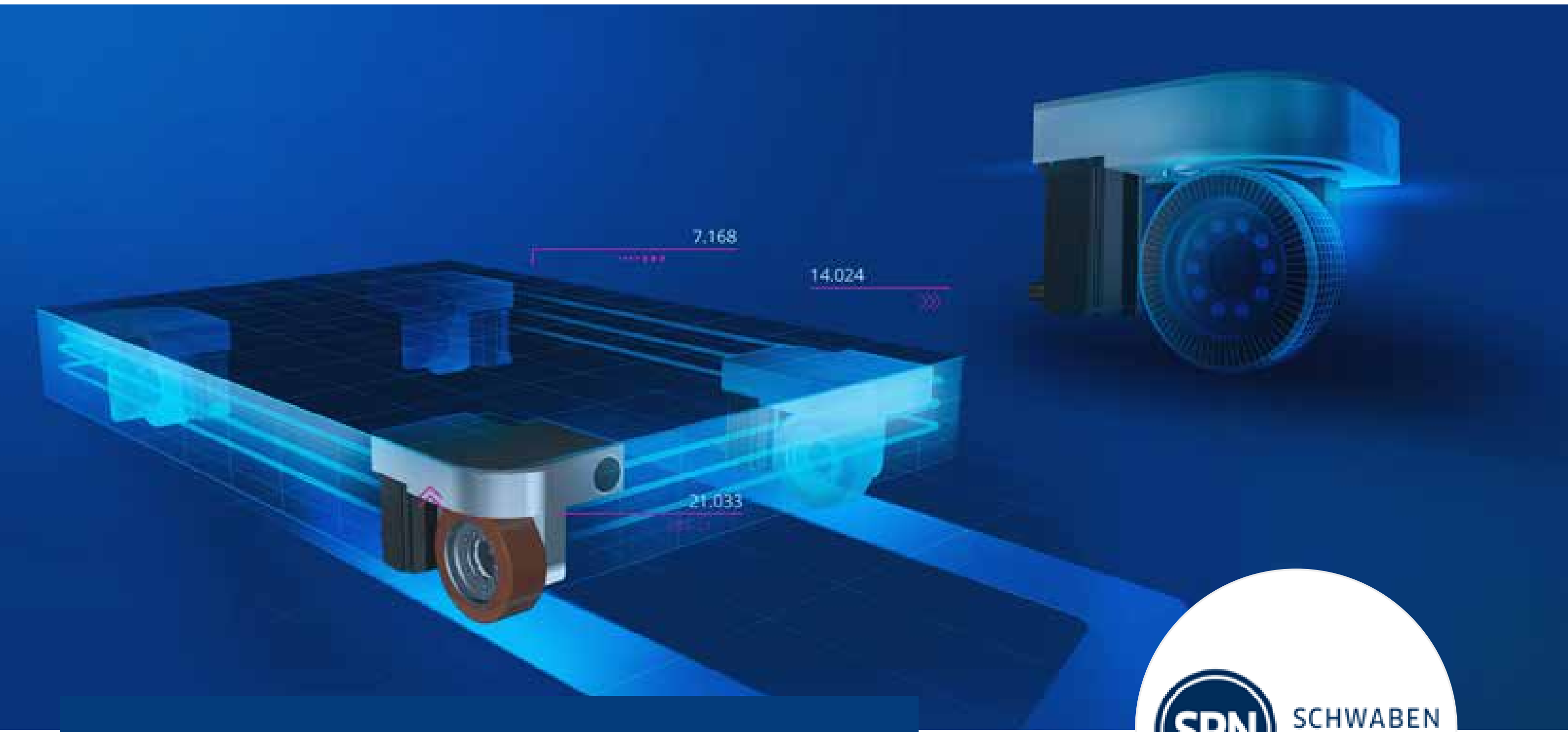

Tips for designing grease-lubricated gearboxes: The SPN steering drive as an example

by Florian Kotz[1], Oliver Belzer[2]
1. SPN Schwaben Präzision - 2. EnginSoft Germany

Developing efficient and durable gearboxes is a key challenge in mechanical engineering. An optimized design is especially important for steering drives because they are subject to high loads and speeds. Lifetime lubrication is often necessary to ensure that the gearbox operates without requiring additional lubrication.

To minimize wear and prevent overheating, the lubricant must be distributed evenly. SPN Schwaben Präzision (SPN) sometimes uses grease in its travel drives for this purpose.

Grease has several advantages: it allows for the use of cost-effective seals; it is less volatile; it remains stable over a longer period of time; and it adheres well to the relevant points, even at low speeds.

Challenges in gearbox design

Using grease also presents unique challenges. The key is determining the optimal amount of grease. Too little grease results in insufficient lubrication, and too much grease reduces efficiency and can cause overheating.

At the same time, the housing must be designed so that the grease is effectively retained at critical points. This requires optimized geometries that guarantee the formation of grease reservoirs and keep the grease in place, even at high speeds.

Simulation-based optimization of lubricant distribution

Simulation-based tools are increasingly being used to overcome the challenges of lubricant distribution in gearboxes. SPN Schwaben Präzision uses the Particleworks software for this purpose. Particleworks is based on the MPS (moving particle semi-implicit) particle-based method. This method accurately simulates the movement, distribution, and heat generation of lubricating grease.

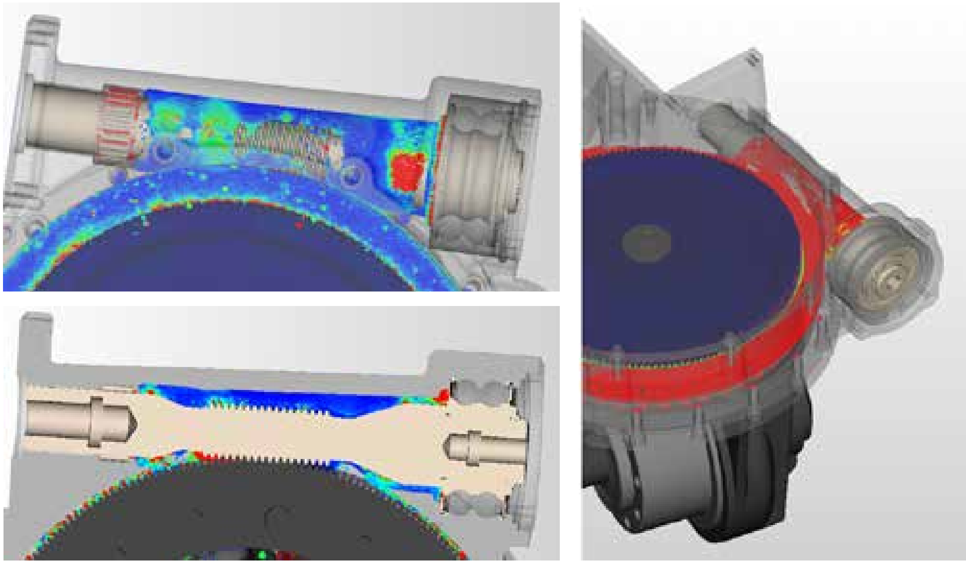

Fig. 1, Fig. 2, Fig. 3. Grease distribution in the simulated steering drive.

The software tracks the movement of individual particles, making it advantageous for simulating complex fluid movements such as lubricant distribution in gearboxes.

In the simulation, the lubricating grease is modelled as a non-Newtonian fluid. Rheological data from the lubricant manufacturer is taken into account, particularly the kinematic viscosity as a function of shear rate. The complete calculation of the Navier-Stokes equations within the software enables precise modelling of the flow dynamics.

Creating grease reservoirs

The simulation results are valuable tools in the field. They enable the selective adjustment of the housing geometry to create grease reservoirs near critical lubrication points, such as tooth flanks and bearings. This optimization process enables pockets, grooves or recesses to be developed to redirect the grease in a targeted manner, ensuring its presence at critical points, even at high speeds.

The simulation results also help to determine the optimal amount of grease. It should be noted that both a lack and an excess of grease can negatively impact gearbox performance. The type of grease used is also crucial. Its kinematic viscosity must meet the demands of high speeds and loads, while ensuring high shear stability in the intended application.

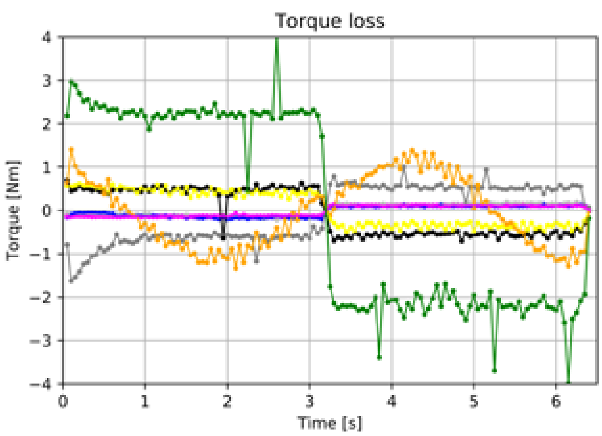

Fig. 4. Torque loss in Nm: with simulations developers can and developers not only the lubrication performance and the service life of a gearbox but also minimize efficiency losses minimize efficiency losses.

Validating simulation results

SPN Schwaben Präzision's testing laboratory conducted physical tests in order to realistically reproduce the demanding simulations associated with lubricating greases. The developers compared grease distribution using transparent housings. The results showed that the simulation accurately replicated real lubricant distribution and grease reservoir formation. In addition, the simulation software parameters were optimized to achieve comparable loss torques for common types of gears.

Using simulations strategically improves lubrication performance and service life in gearboxes while minimizing efficiency losses. The result is better technical performance and reduced overall operating costs, including lower energy requirements.

Conclusion

The purposeful use of this type of simulation improves lubrication performance and the service life of gearboxes, while also minimizing efficiency losses. This results in increased technical performance and reduced operating costs, such as lower energy consumption. Intelligent housing design, an optimal grease quantity, and targeted grease distribution can make travel drives more efficient, durable, and economical.

For more information:
Michele Merelli – EnginSoft
m.merelli@enginsoft.com
Oliver Belzer - EnginSoft Germany for the DACH region
o.belzer@enginsoft.com

About SPN

SPN Schwaben Präzision is a technology-independent gearbox designer with a high-tech production facility in Nördlingen in Germany. Around 300 employees at the Nördlingen headquarters develop and manufacture gearboxes, gearing elements, drive systems, and components for drive technology and mechatronics in a 10,300m² production area. The focus is always on the customer's individual requirements. Drive solutions from SPN are precisely tailored to these requirements, even in small quantities.

Smarter wheels: How multi-physics optimization is shaping the future of automotive design

by Marco Evangelos Biancolini[1], Emanuele Di Meo[2], Riccardo Serenella[2], Claudio Ponzo[3], Sarwar Ahmed[3], Adam Collins[3], Raff Russo[3]
1. University of Rome “Tor Vergata” - 2. RBF Morph - 3. Nissan Technical Centre Europe

In the rapidly evolving field of automotive engineering, designing road wheels is a complex challenge that combines aesthetics, performance, and efficiency. At the 2025 NAFEMS World Congress, a collaborative project involving Nissan Technical Centre Europe, RBF Morph, and the University of Rome “Tor Vergata” presented a cutting-edge methodology that integrates styling, structural integrity, and aerodynamic performance through multi-physics optimization. This approach centres on advanced mesh morphing technology, which is enabled by rbfCAE [1], the latest platform developed by RBF Morph.

Engineering meets aesthetics in the EV era

In the age of electric vehicles (EVs), every gram saved, and every bit of aerodynamic resistance reduced counts. As one of the most visible components of any vehicle, wheels play a key role in mechanical performance and in branding and visual appeal. Electric vehicles place greater demands on wheels than ever: they must be lightweight for extended range, strong enough to withstand varying road conditions, and designed to minimize aerodynamic drag. Meeting these competing demands requires a comprehensive design approach, which is exactly what this research provides.

The study combines simulation tools like finite element analysis (FEA) and computational fluid dynamics (CFD) in a unified workflow. This enables real-time performance feedback and iterative design updates. Mesh morphing with radial basis function (RBF), a technique that applies fluid and continuous shape transformations directly to simulation meshes [2, 3] eliminates the need for traditional remeshing.

A legacy of innovation - the 50:50:50 paradigm

The foundations of this project were laid over a decade ago with the introduction of the 50:50:50 approach [4]: 50 shape variants, 50 million cells, completed in 50 hours. This methodology remains a key part of optimization, particularly as it transitions into AI-supported frameworks. The same principles of high automation, fidelity, and speed underpin the multi-physics workflow used in this study.

This concept has evolved beyond its original scope and now serves as a precursor to reduced-order modelling (ROM) and AI-based design tools. The ability to swiftly produce a substantial dataset of high-fidelity simulations is essential for training surrogate models and interactive dashboards.

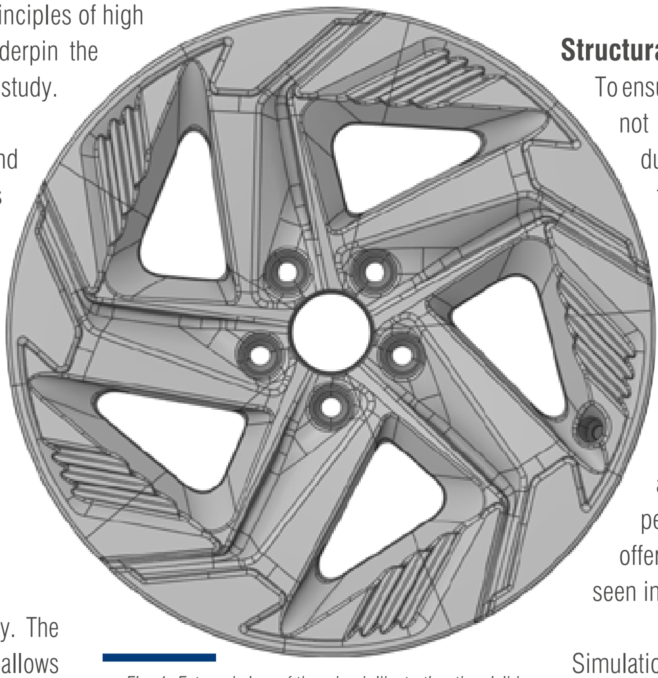

Fig. 1. External view of the wheel, illustrating the visible side that was kept fixed during optimization.

Building the multi-physics workflow

Styling requirements

Wheels define a vehicle's personality. The proposed optimization pipeline allows designers to bring their vision to life without compromising on structural or aerodynamic performance. The rbfCAE platform makes it possible to preserve aesthetic constraints, like spoke curvature or rim contours, while simultaneously modifying geometry for engineering benefits. Fig. 1 shows the outer surface, which corresponds to the visible side of the rim. This was kept fixed throughout the process to preserve its distinctive style, while optimization focused on the inner side of the wheel.

Design and engineering teams can interact through a shared workflow where domain-specific KPIs (key performance indicators) prompt targeted changes, and the impact of each change can be viewed immediately within an integrated visualization environment. This facilitates an informed, iterative process of convergence between CAD styling and CAE validation.

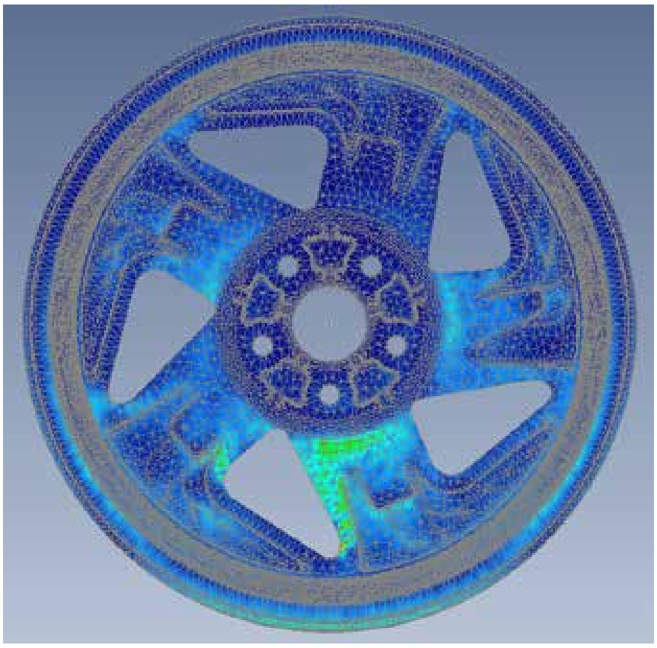

Fig. 2. Von Mises stress results for the baseline wheel configuration.

Structural performance

To ensure that any design modifications would not compromise the product's strength, durability, and impact resistance, a finite element analysis (FEA) was performed using Simcenter Nastran [5]. The wheels were modelled using an AlSi7Mg0.3 aluminium alloy and meshed with second-order tetrahedral elements.

The basic model, consisting of around 260,000 elements, revealed a peak stress well below material limits, offering room for optimization, as can be seen in Fig. 2.

Simulation conditions aligned with virtual certification standards, including static radial load tests, fatigue, and drop tests. The optimization workflow focused on one of the most demanding loading scenarios to ensure structural robustness under worst-case conditions.

Aerodynamics

CFD simulations were performed using HELYX software [6] on an AeroSUV model [7] with the wheel design being considered in this study, in order to measure airflow around the wheel and vehicle body. Note that the estimation of the aerodynamic effect is intended solely for the validation the proposed workflow. For confidentiality reasons, an AeroSUV body was used in place of the original vehicle geometry. The analysis used a steady-state RANS model with the k-ω SST turbulence formulation. The wheels were modelled using the multiple reference frame (MRF) approach to simulate rotation, with over 60 million cells per configuration. This aerodynamic evaluation was crucial in reducing drag and improving the vehicle's overall efficiency.

The use of the arbitrary mesh interface (AMI) method to enable more detailed transient simulations was also explored. Although it was not implemented in this study, the AMI method paves the way for future dynamic evaluations, such as driving simulations with rotating wheels.

Optimization strategies: parametric vs. evolutive

Two optimization routes were explored using the rbfCAE platform:

- Parametric morphing: Shape changes were controlled by user-defined variables, as previously described [8, 9]. Specific internal regions of the rim were offset to ensure compliance with minimum thickness requirements while preserving external styling features. Fig. 3 shows the rbfCAE platform setup for this case. This approach enabled precise tuning of performance attributes.

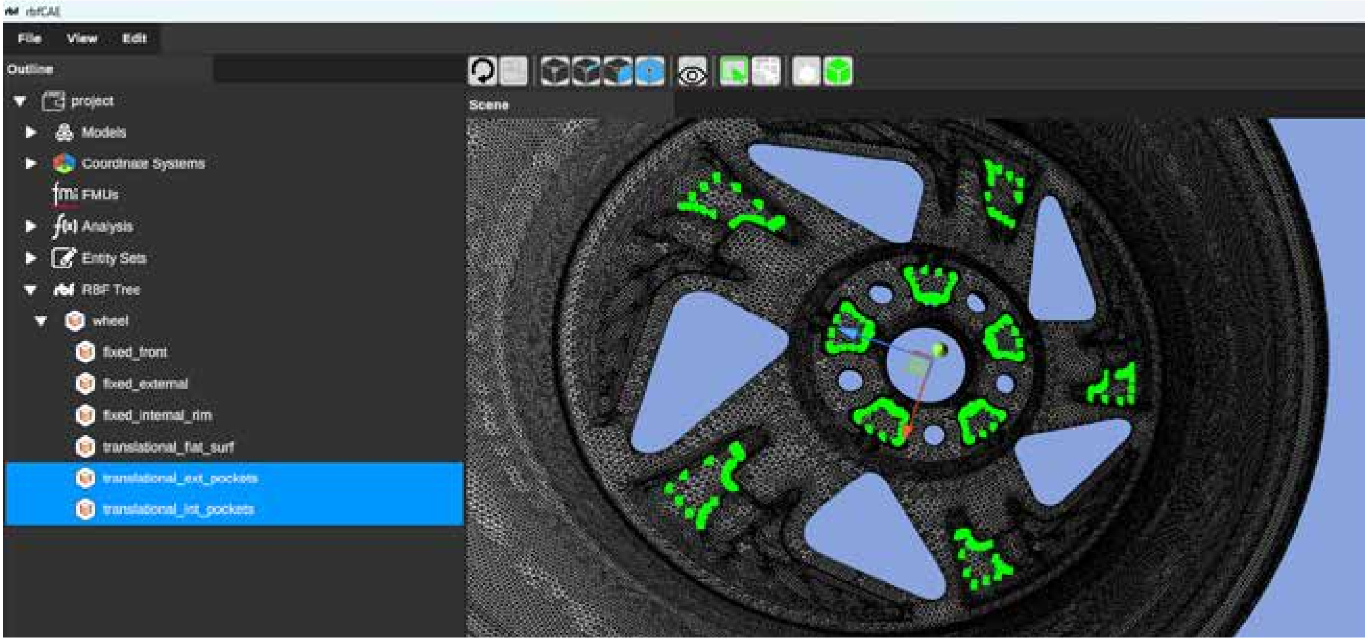

Fig. 3. rbfCAE platform setup for parametric mesh morphing.

- Biological growth method (BGM) morphing: Inspired by how bones and trees grow under stress, this method modifies geometry based on von Mises stress fields [10, 11]. Regions under less stress are thinned out and high-stress areas retain more material. This process yields organic, performance-driven shapes.

The parametric morphing approach is ideal for design studies that require full geometric control and strict style constraints. By contrast, BGM morphing offers a self-regulating mechanism that allows the geometry to adapt naturally to stress.

Case study: from simulation to results

Two optimization strategies were applied to an 18-inch production wheel. A structural analysis revealed that, while maintaining safety, parametric morphing slightly increased peak stresses. Conversely, the BGM design reduced stress concentrations. Both approaches reduced the wheel's mass by 400g.

The optimized designs were then integrated into a complete AeroSUV model and tested at 140km/h in open-air conditions. Table 1 summarizes the differences in drag and lift values, which were analysed to understand their impact on the vehicle's overall aerodynamics. Fig. 4 illustrates this by showing a comparison of the vortex structure (Q) and the 25,000 iso-surface distribution.

Configuration	FEMFAT WELD method	Von Mises stress (MPa)	Drag coefficient	Lift coefficient
Baseline	14.1	78.1	0.302	-0.013
Parametric morphing	13.7	81.3	0.304	-0.025
BGM morphing	13.7	75.9	0.305	-0.021

Table 1: Comparison of results between baseline and morphed configurations.

Although there is a slight increase in drag, the increased downforce and reduced mass could result in significant performance improvements, particularly for EVs that rely on regenerative braking and low rolling resistance.

rbfCAE: the engine behind the innovation

The rbfCAE platform enabled design changes to be seamlessly integrated into the FEA and CFD simulations. Avoiding remeshing significantly reduces the time required for each iteration. Thanks to its automated workflow manager, parametric tree setup, and connectors to solvers such as Simcenter Nastran and HELYX, the platform is the perfect tool for high-fidelity, cross-domain optimization.

The morphing tree structure enabled hierarchical and reversible modifications, supporting both global design changes and localized refinements. Each branch of the tree represented a parametric dependency, enabling engineers to trace and refine every transformation.

From morphing to real-time optimization

A clear path has been outlined for integrating reduced order models (ROMs) and artificial intelligence (AI) into the workflow. RBF Morph has already demonstrated these capabilities in the automotive field by enabling real-time geometry manipulation through interactive design dashboards and VR tools [12].

Other examples include using ROMs to optimize the aerodynamics of a cyclist's helmet [13] and developing a VR-based aircraft design environment [14]. In the latter example, mesh morphing combined with real-time feedback significantly accelerated the design loop.

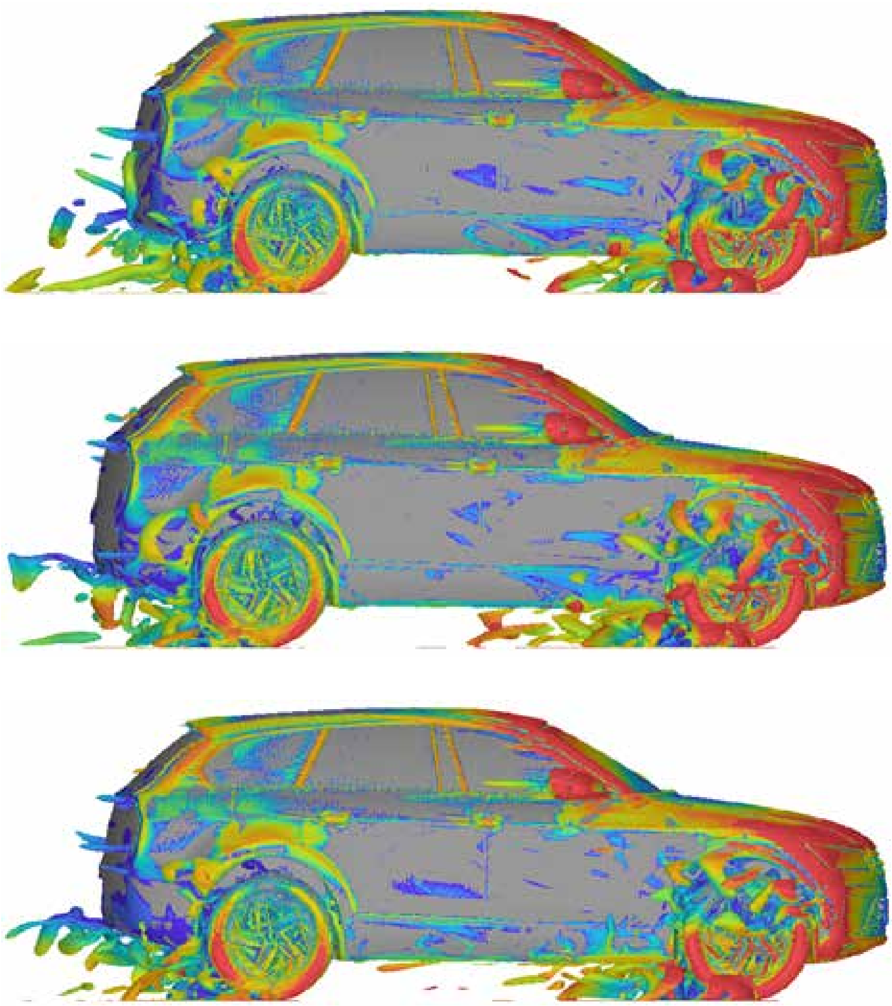

Fig. 4. Vortex structure (Q): 25,000-iso surface distribution, coloured by mean velocity, for the baseline (a), parametric-morphed (b), and BGM morphed (c) wheel configurations.

Conclusion

This work sets a new standard for automotive wheel design, facilitating collaboration between engineers and designers via a digital, multi-physics platform. By integrating simulation, mesh morphing, and optimization into one process, we demonstrated how to optimize performance, efficiency, and aesthetics. As vehicles continue to evolve, especially toward electrification, tools like rbfCAE will be essential for overcoming new design challenges.

The future of automotive design is lighter, smarter, and more integrated. It starts with the wheels.

RBF Morph, the University of Rome “Tor Vergata”, and Nissan jointly presented this pioneering work at the 2025 NAFEMS World Congress, showcasing their shared vision for an integrated, simulation-driven approach to automotive design.

For more information:
Emanuele Di Meo - RBF Morph
emanuele.dimeo@rbf-morph.com

References

[1] RBF Morph, “Our RBF Morph Technology” [online], accessed 20 June 2025, available at: rbfcae.com/our-rbfcae-technology/

[2] A. van de Boer and H. Bijl, “Mesh deformation based on radial basis function interpolation”, *Computers & Structures*, vol. 85, no. 11–14, June 2007, pp. 784–795, doi.org/10.1016/j.compstruc.2007.01.013

[3] M. E. Biancolini, “Mesh Morphing and Smoothing by Means of Radial Basis Functions (RBF)”, *Handbook of Research on Computational Science and Engineering: Theory and Practice* (pp. 347–380), edited by J. Leng and Wes Sharrock, IGI Global Scientific Publishing, Hershey, PA, USA, 2012, doi.org/10.4018/978-1-61350-116-0.ch015

[4] A. Khondge and S. Sovani, “An Accurate, Extensive, and Rapid Method for Aerodynamics Optimization: The 50:50:50 Method”, SAE Technical Paper 2012-01-0174, Apr. 2012, doi.org/10.4271/2012-01-0174

[5] Siemens Digital Industries Software, Simcenter Nastran Software [online], accessed 20 June 2025, available at plm.sw.siemens.com/en-US/simcenter/mechanical-simulation/nastran/

[6] ENGYS, HELYX, “Open-Source CFD for Enterprise” [online], accessed 20 June 2025, available at: engys.com/helyx/

[7] European Car Aerodynamic Research Association (ECARA), AeroSUV – ECARA, [online], accessed 20 June 2025, available at: ecara.org/drivaer-1

[8] S. Porziani, C. Groth, H. Zhang, and M. E. Biancolini, “Advancing Structural Optimization of an Electric Motor Rotor through Mesh Morphing Techniques,” IOP Conference Series Materials Science and Engineering, vol. 1306, no. 1, May 2024, pp. 012033–012033, doi.org/10.1088/1757-899x/1306/1/012033

[9] U. Cella, D. Patrizi, S. Porziani, T. Virdung, and M. E. Biancolini, “Integration within Fluid Dynamic Solvers of an Advanced Geometric Parameterization Based on Mesh Morphing”, *Fluids*, vol. 7, no. 9, Sep. 2022, p. 310, doi.org/10.3390/fluids7090310

[10] S. Porziani, C. Groth, W. Waldman, and M. E. Biancolini, “Automatic shape optimisation of structural parts driven by BGM and RBF mesh morphing”, *International Journal of Mechanical Sciences*, vol. 189, Jan. 2021, p. 105976, doi.org/10.1016/j.ijmecsci.2020.105976

[11] C. Mattheck and S. Burkhardt, “A new method of structural shape optimization based on biological growth”, International Journal of Fatigue, vol. 12, no. 3, May 1990, pp. 185–190, doi.org/10.1016/0142-1123(90)90094-u

[12] RBF Morph, “Interactive Aerodynamic Development in VR” [online], YouTube video, accessed 20 June 2025, available at: youtube.com/watch?v=kprO2k3uSgY

[13] E. Di Meo, A. Lopez, C. Groth, M. E. Biancolini, and P. P. Valentini, “Reduced-Order Model of a Time-Trial Cyclist Helmet for Aerodynamic Optimization Through Mesh Morphing and Enhanced with Real-Time Interactive Visualization”, *Fluids*, vol. 9, no. 12, Dec. 2024, p. 300, doi.org/10.3390/fluids9120300

[14] A. Lopez and M. E. Biancolini, “Development of a Reduced Order Model-Based Workflow for Integrating Computer-Aided Design Editors with Aerodynamics in a Virtual Reality Dashboard: Open Parametric Aircraft Model-1 Testcase”, *Applied Sciences*, vol. 15, no. 2, Jan. 2025, p. 846, doi.org/10.3390/app15020846

Thermo-fluid dynamic simulation of hot isostatic pressure quenching (HIPQ) on aircraft blades

by Paola Brambilla[1], Nicola Gramegna[1], I. Mondino[2], M. Coppola[2], M. Sabella[2]
1. EnginSoft - 2. Avio Aero

Hot Isostatic Pressing (HIP) is an established technology in the aerospace industry used to develop and produce alloys for high-performance applications such as turbine rotor blades.

HIP is increasingly being used in additive manufacturing (AM) technologies for metallic materials because it reduces the defects typical of these new technologies, thereby significantly increasing the performance of new materials developed for AM. However, HIP systems typically cannot guarantee specific control of the cooling phases and therefore post-HIP heat treatments are commonly used on AM-produced materials to transform their microstructure to the required standards.

This paper studies the latest generation of HIP systems, known as HIP/quench (HIPQ) systems, which combine the HIP process and subsequent controlled cooling in a single system to simultaneously reduce defects and achieve the desired microstructure in a single thermal cycle, with obvious reductions in cost and production time. This paper investigates a combined HIPQ cycle applied to turbine blades produced by additive electron beam melting (EBM) technology for titanium aluminium alloys (Ti48Al2Cr2Nb).

The HIPQ treatment simulation analyses and determines how to optimize the temperature and distribution of airflow within the furnace to ensure a uniform temperature across all blades regardless of their position in the chamber, and to reduce thermal gradients during the immersion and cooling phases. This avoids microstructural variations in the blades as a result of their position in the furnace thus maximizing their mechanical properties.

The study examines a number of design parameters, including furnace geometry, basket and blade arrangement, and the air flow generated by the centrifugal fan. The results show how this simulation approach can analyse the efficiency of the heat treatment process helping to improve the performance and durability of critical aerospace components. Understanding the thermo-fluid-dynamic details also reduces the design of experiments to a minimum while improving the final quality of the material.

This paper discusses the application of computational fluid dynamics (CFD) to the verification of the furnace selected to combine the HIP and controlled cooling process of turbine blades for aeronautical engines produced with additive technology.

The activities described were carried out as part of the SIADD project co-financed by the National Operational Program (PON) "Research and Innovation 2014-2020" with MIUR code no. 1735 of 07/13/2017. We would like to thank all project partners for their fruitful cooperation: DTA– Aerospace Technology District (lead partner), ELFIM, ENEA, EnginSoft, GE AVIO, HB Technology, Ingenia, ITIACNR, CNR, Novotech, Polytechnic of Bari, Polytechnic of Milan, UMBRA Group Cuscinetti, University of Enna "KORE", and University of Salento. SIADD is the Italian abbreviation a Ministry of Instruction and Research-sponsored project focusing on innovative solutions for quality and sustainability in additive manufacturing processes.

Hot isostatic pressure quenching (HIPQ)

Hot isostatic pressing (HIP) is an established technology in the aerospace industry for developing and producing materials for high-performance applications, such as turbine rotor blades. This HIP process combines high temperature and pressure to densify materials, eliminating porosity and other structural defects introduced during the manufacturing process and improving mechanical properties, particularly fatigue strength and ductility.

HIP is proving to be increasingly indispensable, especially in additive manufacturing (AM) technologies for metallic materials where it reduces the defects typical of these new technologies, significantly increasing their performance and making them competitive with conventionally produced products.

In addition to hot isostatic pressing, AM components require heat treatment to further improve their microstructure and hence mechanical properties. At present, HIP systems cannot generally guarantee detailed control of the required cooling rate after heat treatment, which means that the materials require additional specific heat treatment in a different furnace after HIP.

It is therefore essential to investigate the post-processing of AM-produced titanium-aluminium (TiAl) alloy components in the latest HIP systems, namely HIP/Quench (HIPQ), which promise to combine high pressures and controlled cooling in a single system, thus successfully combining the post-production treatment of items currently produced in different equipment and often different facilities.

HIPQ systems could effectively simplify and optimize current AM production processes, significantly reducing existing production cycle times. In addition, the ability to combine pressure and controlled cooling in the same system promises to deliver equal or better results in terms of microstructure and mechanical properties than the separate processes usually used.

This paper focuses on TiAl turbine rotor blades manufactured using the EBM (electron beam melting) AM process and subsequently subjected to the combine HIP and heat treatment (HIP/Quench) process.

CFD simulations of heat flows within a furnace are an established practice for investigating and optimizing the furnace and its potential heat treatment capabilities. Geometrical discretization and material modelling allow the simulation of different usage scenarios, varying the boundary conditions to identify the ideal configuration that provides the most homogenous heating and cooling of the numerous blades arranged on two levels.

This article describes the assumptions used to model argon gas and analyses the results at key points in the process.

In this study, particular attention was also paid to numerically simulating the environment and the HIPQ treatment with CFD techniques in order to facilitate the definition of optimal process parameters and simulate their impact on materials.

This will simplify the transition from laboratory environment to industrial-scale development.

This activity was part of a larger project, SIADD, that not only aimed to optimize the HIPQ process, but also to study different materials and processes that harness additive technology.

The use case

Avio Aero provided low pressure turbine (LPT) blades made of TiAl alloy using EBM additive manufacturing technology to test the HIPQ process on real aircraft components. The nominal composition of

Fig.1. Example of EBM LPT blades before any HT.

the alloy is Ti-48Al-2Cr-2Nb [reference: US patent 4,879,092].

The test case was analysed in terms of microstructure, mechanical properties, thermal distortion, and porosity closure effectiveness to verify the impact of the proposed HIPQ cycle compared to the standard process (separate HIP and HT cycles). The homogeneity of the furnace over the entire working volume was studied at all stages of the HIPQ cycle, demonstrating the ability of the process to produce a uniform alloy microstructure and hence uniform mechanical properties in all positions of the chamber.

Porosity closure efficiency and blade thermal distortion were also studied in comparison with standard HIP and HT cycles in order to exclude any different behaviours when combining HIP+cooling rates in the same cycle (for example, risk of pore reopening during cooling).The simulation of HIPQ cycle allowed us to identify the worst position in the chamber in terms of temperature uniformity, especially during the transient phase, and to selectively study the worst positions in order to define better HIPQ parameters.

Simulation of HIPQ

Geometrical model and grid

The geometric model of the furnace, shown in Fig.2, represents the actual structure of the treatment system in which the blades are arranged on two levels (upper and lower) of the basket. The accuracy of the mesh in three-dimensional space is essential to capture the flow and temperature variations in the gaps between the different blades. The quality of the overall model developed was confirmed by interpolating virtual sensors and comparing their temperature-time curves with real thermocouple curves.

The virtual sensors for monitoring the temperature in specific areas of the furnace consist of thermocouples inserted in blocks (55mm x13mm x13mm) made of the same material as the blades. These blocks were also faithfully modelled in the numerical simulation. The table shows the positions of the four sensors considered: WL02, WL07, WL08, WL09 (Fig.3)

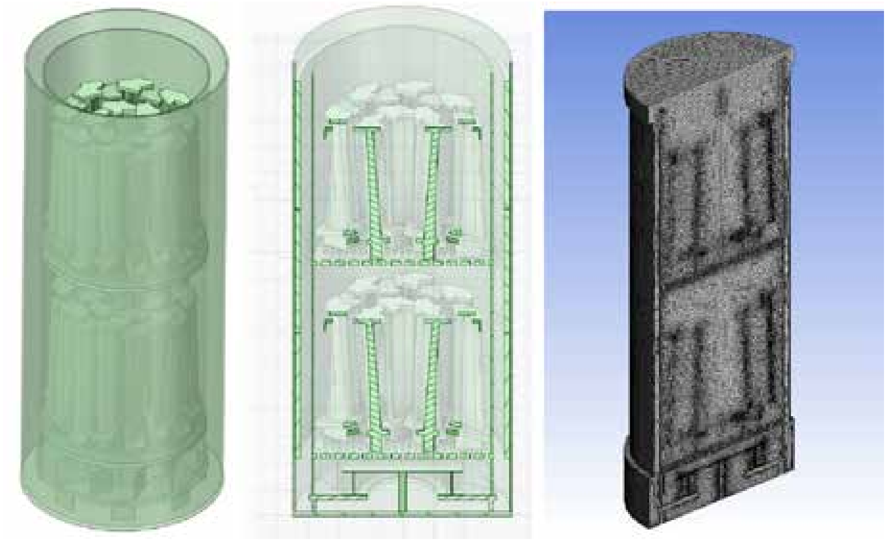

Fig.2. CFD model (left) and vertical section of the mesh including blades (right).

To simulate the thermal cycle under study, the reference curve of the WL08 probe was replicated. The temperature curves collected from the other probes were used to verify the reliability of the replication of the actual thermal cycle. The fan was explicitly modelled using the Frozen Rotor approach, which allows the flow that develops around the fan to be accurately evaluated without simulating its relative movement with respect to the static diffuser. This saves computational time without sacrificing accuracy.

All solid domains inside the furnace (load plates, furnace structure, basket, static diffuser) were modelled taking into account the thickness of each individual component to calculate the thermal inertia.

The electrical resistors that heat the argon for the HIP phase were modelled as heat sources applied to the internal furnace walls. The glycol water flowing outside the furnace for the quench phase was modelled as an energy sink applied to the internal furnace walls. The fluid domain of the furnace coincides with the argon volume.

Material modelling and boundary conditions

The thermo-fluid dynamics analysis was performed using the Ansys CFX 2021 R1 solver [1]. The shear stress transport (SST)

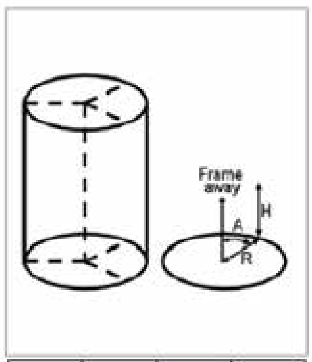

ID	R [mm]	H [mm]	A [°]
WL02	180	965	60
WL07	0	965	90
WL08	10	520	90
WL09	10	35	90

Fig.3. Photo of the oven (courtesy of Pres-X) and the positions of the sensors.

Al	Cr	Nb	Fe	C	O	N	H	Ti
32.0-33.5	2.2-2.6	4.5-5.1	Max. 0.05	Max. 0.025	Max. 0.12	Max. 0.02	Max. 0.003	Bal

Table 1. Chemical composition of aluminium and titanium alloy for the blades.

turbulence model and the discrete transfer model radiation models were used. Energy resolution within the different solid and fluid domains was enabled. For the fluid, argon was modelled as a real gas through the Peng-Robinson equation of state, formulated as follows:

$$p = \frac{RT}{v-b} - \frac{a(T)}{v^2 + 2bv - b^2}$$

where

$$b = 0.0778\frac{RT_c}{p_c}$$

$$a(T) = a_0(1 + n(1 - \sqrt{\frac{T}{T_c}}))^2$$

$$a_0 = 0.45724\frac{R^2T^2{}_c}{P_c}$$

The factor n is calculated as a function of the eccentricity factor w

$$n = 0.37464 + 1.54226w - 0.26993w^2$$

The blade material is an aluminium and titanium alloy as shown in Table 1.

The density of this TiAl material is 0.144lbm/in^3. Specific heat and thermal conductivity vary with temperature.

The furnace material is molybdenum with the following properties:

- Density =10,200kg/mc
- Specific heat $[Cal/Kmol] = 5.69+0.00188T- (50300/T^2)$
- Thermal conductivity $[W/mK] = 8*10^{-6}T^2- 0.0491T+152.32$

In both phases, the fan does not have a constant speed, but a constant speed assumption was applied in agreement with the partners. The value imposed is the average value calculated for each phase. In the HIP phase, the fan rotates at an average speed equal to 30% of the maximum speed. In the quench phase, the speed increases to 80% of the maximum speed. Since the maximum speed is 900rpm, the fan speed is 270rpm in the HIP phase and 720rpm in the quench phase. The heating elements in the HIP phase and the glycol water in the quench phase were modelled as heat sources and sinks, respectively, associated with the internal furnace walls. Heating and cooling were modulated to follow the temperature trend detected by the WL08 thermocouple positioned in the centre of the furnace during the experimental phase.

Project results

Simulation and actual results

In the present study, a numerical simulation of a typical HIP-Quench cycle is presented. The heat treatment parameters were selected after several laboratory-scale tests. Once the optimized parameters were identified, a new industrial-scale test campaign was carried out to confirm the preliminary results obtained in the laboratory in terms of material properties, porosity closure, and dimensional distortions, which are in line with expectations and comparable to conventional heat treatments.

A numerical simulation was carried out using CFD techniques, focusing specifically on the heating and cooling phases of the entire HIPQ treatment. The output was the thermal distribution inside the furnace to verify the temperature uniformity for each blade. Of interest is the good uniformity observed in the temperature distribution on each component as well as within the entire furnace volume. For example, at the end of the heating phase, a maximum difference of 5°C can be detected between the coldest and hottest point of the blades (Fig.4).

The temperature range during heating corresponds to the minimum and maximum temperature values measured at the time displayed. This range makes it possible to better highlight the temperature gradients that develop on each blade at each instant.

The red areas highlight higher temperatures, while the blue areas correspond to areas with lower temperatures. The cross-sections of the upper basket (Fig.5) show the temperature distribution at 65 and 130 minutes of the heating phase. Six numbered blades were used as a reference to check the temperature homogeneity and the effect on the microstructure.

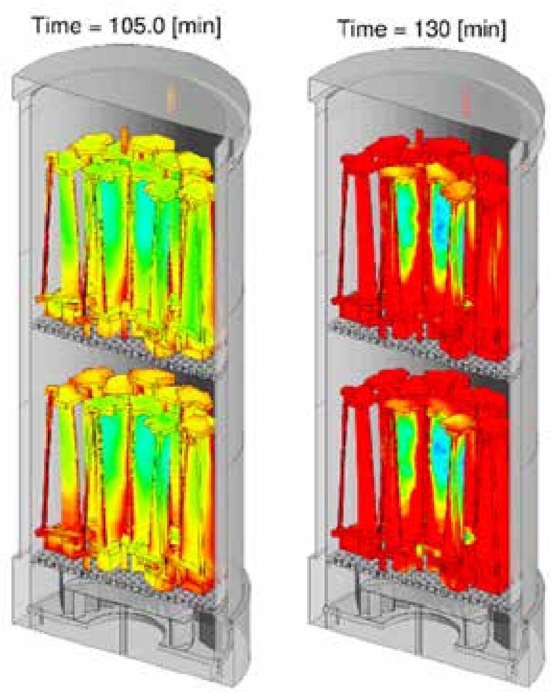

Fig. 4. Heating: Examples of temperature mapping from CFD analysis.

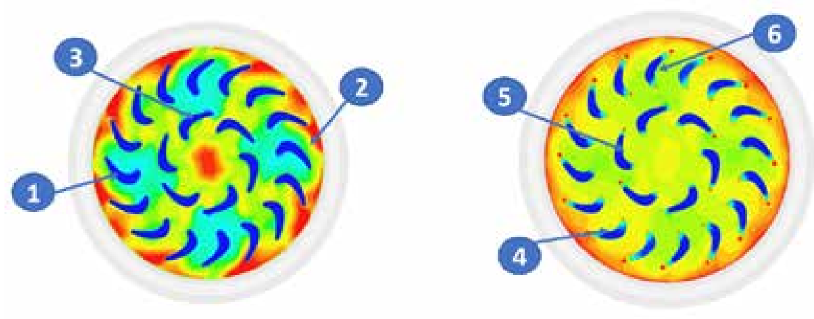

Fig. 5. Heating temperature distribution at 65 min and 130 min in the upper basket; test numbers and locations inside the containers.

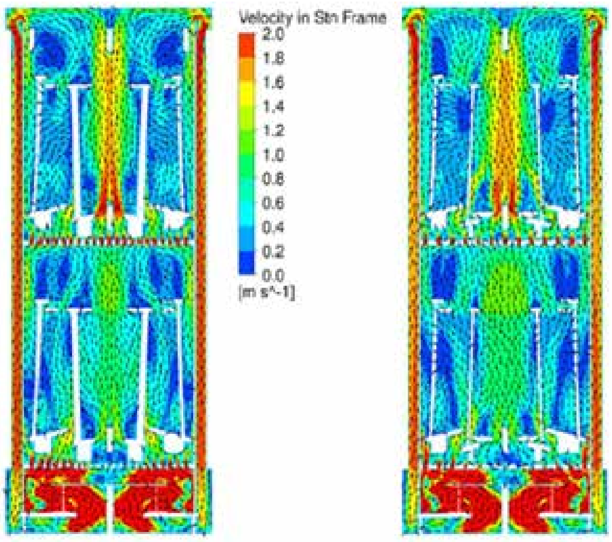

Fig.6. Quench: Flow distribution and velocity vectors.

Fig. 6 shows that the areas where the flow recirculates (area under the roof) or the areas in the wake of obstacles such as the dovetail are the areas with the highest temperature. The velocity contour and the velocity vectors are shown on two mid-levels of the oven section. Since the velocity field does not vary during the steady state thermal cycle, a single instant was considered as an example. The velocity in the middle area of the upper basket is higher than any other area of the furnace.

Experimental results

The simulation results were confirmed by the experimental data collected on the test parts treated in this furnace cycle: six out 40 blades, three from each basket, were inspected and tested. Microstructural analysis, tensile tests on specimens taken from blade, porosity and dimensional inspections (both by CT scanning) were performed to verify that the effect of the HIPQ treatment was equivalent to that of conventional heat treatment in terms of mechanical and material properties. This study also demonstrated high temperature uniformity within the furnace (Fig.7). Computer tomography (CT) was performed before and after HIPQ treatment for both dimensional and porosity inspection. No distortion anomalies or typical defects were detected. After CT inspection, cutting showed that the microstructure of each blade examined was the same as the typical microstructure found on the standard material. No anomalies or microstructural differences were detected among the samples analysed. In addition, the data collected is in line with the standard values obtained from the conventional process consisting of two different heat treatments, HIP, and heat treatment (Fig. 8).

A tensile test at room temperature was performed on each blade analysed and the results are shown in the graphs in Fig.9a–c.

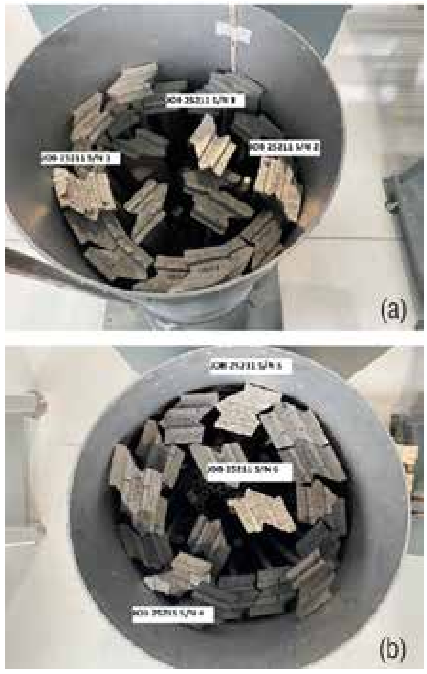

Fig. 7. Example of blades inside the furnace baskets: (a) lower basket and (b) upper basket.

The blades show the same behaviour in terms of mechanical properties.

Conclusions

A HIPQ treatment simulation was used to analyse and then determine how to optimize the temperature and distribution of airflow within the furnace to ensure a uniform temperature across the treated components, regardless of their position in the chamber, and to minimize the thermal gradients during the heating and cooling phases. This minimizes the variation in

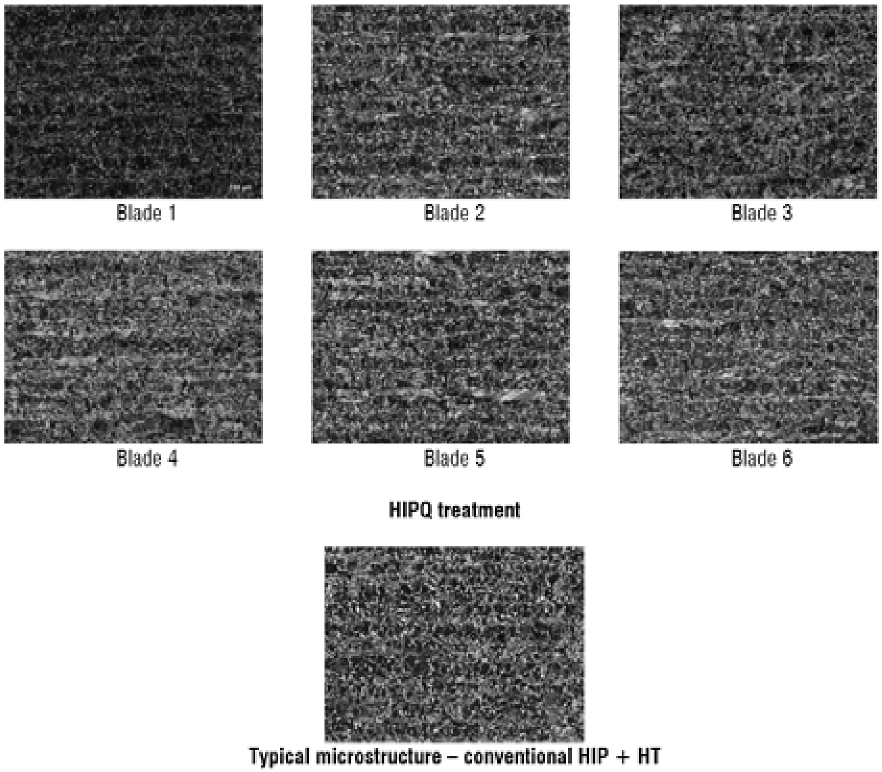

Fig.8. Analysis of six HIPQ microstructures (100x) and comparison with a conventionally produced structure.

References

[1] *Ansys CFX-Solver Theory Guide* (release 2021-R1), Ansys Inc., Canonsburg, PA, USA, 2021.

[2] R. Perry and D. Green, *Perry's Chemical Engineers' Handbook,* sixth edition, McGraw-Hill: New York, 1985.

[3] Quintus Technologies, *Quintus Technologies' Heat Treatment* [Online]. Available: quintustechnologies.com/hot-isostatic-pressing/applications/heat-treatment/.

[4] W. H. Peter and et al, *Understanding the Role of Hot Isostatic Pressing Paramters on the Microstructural Evolution of Ti-6Al-4V and Inconel 718 Fabricated by Electron Beam Melting,* Oak Ridge National Laboratory, Oakridge, TN, USA, Mar. 2015, doi: 10.2172/1209206

[5] S. Mashl, A. Eklund, and M. Ahlfors, "Rapid High Pressure Gas Quenching During HIP: Combining Densification and Heat Treatment into a Single Process," in European Congress and Exhibition on Powder Metallurgy, European Powder Metallurgy Conference Proceedings; The European Power Metallurgy Association, Shrewsbury, UK, 2016.

[6] F. X. Zimmerman and C. Bergman, "Hip quenching - A Heat Treating Method," in the Second International Conference on Quenching and the Control of Distortion, Cleveland, OH, USA, 4–7 Nov, 1996.

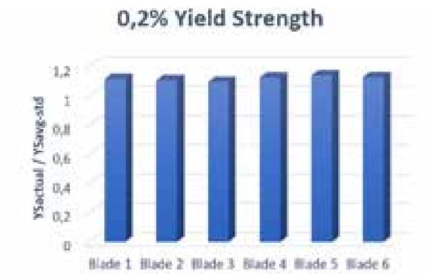

Fig.9 (a). Yield strength deviation for the six blades studied.

Fig.9 (b). UTS deviation for the six blades studied.

Fig.9 (c). Elongation deviation for the six blades studied.

the microstructure of the blade at different locations and, as a result, maximizes the mechanical properties.

Simulation makes it possible to identify optimized parameters to achieve a uniform temperature inside the furnace, thus avoiding material nonconformity and reducing the number of experimental tests required to achieve the optimal set of parameters. This approach can be useful in reducing the time, and therefore cost, associated with feasibility steps and can accelerate process qualification.

The study demonstrates the importance of processing TiAl AM components with the latest HIP systems, known as HIP/Quench, which combine high pressure and controlled cooling in a single system, reducing the time and costs associated with the need to use different equipment and often different facilities. These systems can effectively simplify and optimize current manufacturing processes for AM components, significantly shortening current production cycles.

For more information:
Nicola Gramegna – EnginSoft
n.gramegna@enginsoft.com

About Avio Aero

Avio Aero is a GE Aerospace company that designs, manufactures and maintains components and propulsion systems for civil and military aviation. Today, the company provides its customers with innovative technological solutions to quickly respond to the continuous changes required by the market: additive manufacturing, rapid prototyping, as well as technologies dedicated to the production of transmissions, turbines, and combustors. The company's head office is in Rivalta di Torino, where its largest production facility is also located. Other important facilities are situated in Brindisi and Pomigliano d'Arco (Naples), with a total of around 4,800 employees employed in Italy.

High-fidelity CFD workflow for optimizing wind-assisted propulsion systems

by Giorgio Provinciali[1], Kevin Charpot[1], Tina Črnigoj Marc[2]
1. Oceanwings - 2. Arctur

Oceanwings, a French SME, develops Oceanwings,® an articulated wingsail system that significantly reduces fuel consumption and greenhouse gas emissions for maritime transport. To optimize the Oceanwings system for different vessel types and sizes, the SME required a high-fidelity aerodynamic evaluation method adaptable to a wide range of configurations. Traditional CFD tools were limited in terms of licensing costs, workflow automation, and scalability.

As part of the FF4EuroHPC experiment, a new OpenFOAM-based workflow was developed in collaboration with the Polytechnic of Milan (PoliMi), CINECA, and ToolsPole. This integrated a customized command-line interface to automate large-scale CFD simulations on HPC systems. It replaced GUI-based processes with a fully programmable, batch processing-oriented system.

A rich dataset of aerodynamic performance parameters was generated within a broad design space, requiring over 350,000 CPU hours. Each configuration involved the use of steady-state RANS simulations using the SST k-omega turbulence model and optimized meshing and calculation strategies in a parallelized manner. The domain topologies and boundary conditions were then modified to reflect realistic wind angles and vessel interactions.

We integrated the CFD results into the BREVA platform from ToolsPole. The platform combines simulation results with a Bayesian optimization engine developed by USI. This enabled us to identify the optimal trim parameters for the Oceanwings and maximize aerodynamic thrust under various wind conditions.

Oceanwings has streamlined the CFD-HPC workflow enabling the company to analyse thousands of configurations per vessel in days instead of weeks without relying on commercial software licenses. This allows the company to provide customized sail configurations for yachts, cargo ships, and hybrid vessels, and to supply its AI-based control software with high-fidelity aerodynamic data.

As a result, Oceanwings expects its control algorithms to improve the aerodynamic efficiency of the Oceanwings product by about 10%. This solution enables faster design iterations, improved responses to customer specifications, and a compelling business case for entering new ship categories. The experiment demonstrates how open-source tools and HPC infrastructure can provide SMEs engaged in maritime innovation with democratic access to advanced simulation capabilities.

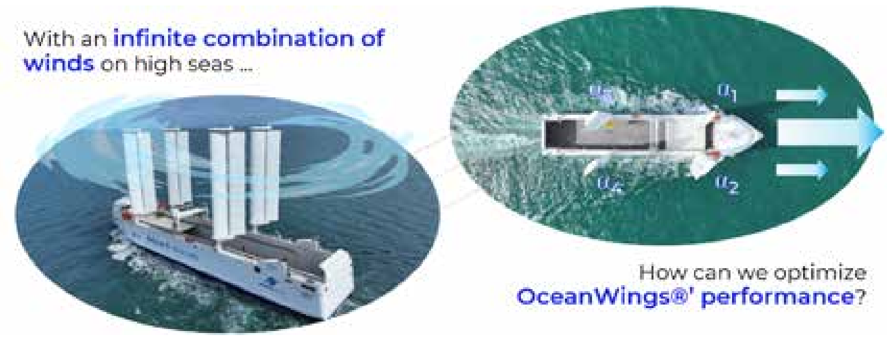

Fig. 1. The challenge of optimizing wind propulsion at sea. This real photograph shows a vessel equipped with four Oceanwings, surrounded by different wind directions. It highlights the combinatorial complexity of optimizing performance at sea.

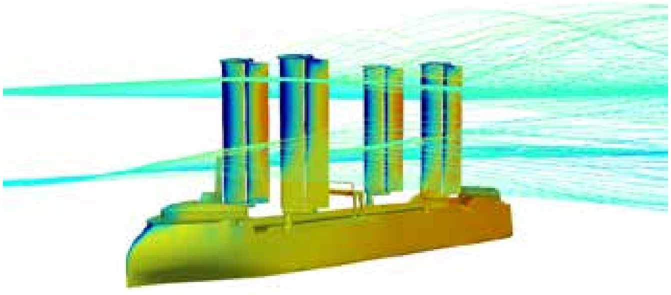

Fig. 2. CFD analysis of the flow lines around the Oceanwings. A visualization of the airflow around a vessel equipped with four Oceanwings, displaying the flow lines and pressure curves at an apparent wind angle of 30°. It demonstrates the realistic aerodynamic interactions between the sails and the superstructure.

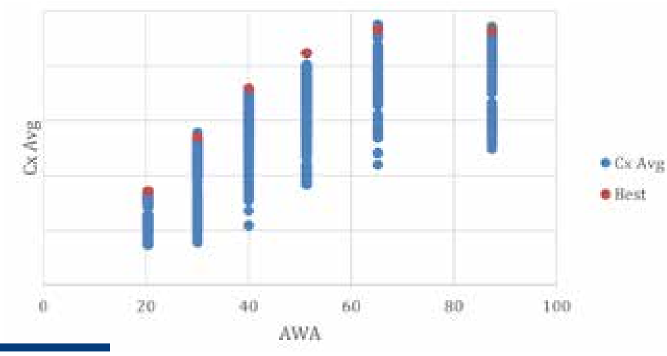

Fig. 3. Thrust coefficient vs. apparent wind angle. This graph shows the average non-dimensional thrust (Cx) coefficient in relation to the apparent wind angle for different trim configurations. The optimal configuration is highlighted to demonstrate the significant performance improvement that can be achieved through optimized trimming.

The success story presented in this article was developed during the first tranche of the FF4EuroHPC Project. FF4EuroHPC supports the competitiveness of European SMEs by funding business-oriented experiments and promoting the adoption of advanced HPC technologies and services. The experiment is an end-user-relevant case study demonstrating the use of cloud-based HPC (high-performance computing) and its benefits to the value chain (from end-user to HPC-infrastructure provider) to address SME business challenges requiring the use of HPC and complementary technologies such as HPDA (high performance data analytics) and AI (artificial intelligence). The successful completion of the experiment has created a success story that can inspire the industrial community.

For more information:

Tina Crnigoj Marc - Arctur; FFplus Communication lead
tina@arctur.si

The FF4EuroHPC project has received funding from the European High-Performance Computing Joint Undertaking (JU) under grant agreement No. 951745. The JU receives support from the European Union's Horizon 2020 research and innovation programme and from Germany, Italy, Slovenia, France, and Spain. FFplus project has received funding from the European High-Performance Computing Joint Undertaking (JU) under grant agreement No 101163317. The JU receives support from the Digital Europe Programme.

The FFplus project has released its second open call for business experiments for SMEs and startups

Throughout the project, SMEs and start-ups will receive support through six funding calls for business experiments (Type 1) and for innovation studies (Type 2).

The business experiments aim to encourage SMEs to adopt high-performance computing (HPC) to address specific business challenges, even if they have no prior experience with HPC services.

The resulting sub-projects will perform "business experiments" that demonstrate to the broader European SME ecosystem how HPC adoption solves business problems and positively impacts businesses through the use of HPC-based computational methods. The key outputs will be success stories that promote, communicate, and disseminate the business impact of HPC adoption within the SME ecosystem.

Proposals are sought that address the business challenges of European SMEs in various application domains. SMEs whose adoption of advanced HPC services will have the greatest business impact will be prioritized. SMEs with an academic focus or that only have long-term potential are outside the scope of this call.

Key call details

Submission deadline: August 26th, 2025 at 17:00 Brussels local time

Expected duration of experiments: maximum of 15 months with a targeted commencement date of January 1st, 2026

The total budget for all sub-projects funded through this call is €4 million.

Several funding constraints and eligibility conditions apply. For more information, see the full announcement on the project website www.ffplus-project.eu.

BeHAP: Automating busbar joule-heating analysis with Ansys Mechanical

by Jae-won Kim
Tae Sung S&E

Batteries are typically made up of cells, modules and packs. Busbars are components that transfer energy between cells or modules. While they perform the same function as wires, their large cross-sectional area makes them more electrically efficient: even though the same current flows, the current density is minimal, reducing heat generation and improving handling.

To maximize these advantages and develop optimal busbar designs, numerous studies are being conducted using analytical approaches that consider factors such as geometry, materials, and current levels. This article describes the thermo-electrical analysis process using Ansys Mechanical and introduces the busbar thermal-electric analysis automation program.

Electric vehicles use high-voltage batteries that can store energy at a high density and consist of several secondary cells to store energy. Multiple secondary cells are connected in series and in parallel to create a battery module. Several modules are then combined into a pack, which is mounted under the vehicle. Busbars are used to efficiently transfer energy between battery cells or modules.

This article will examine the numerical models required for thermoelectric analysis and explain how to perform a busbar thermoelectric analysis using Ansys Mechanical. Busbar thermoelectric analysis requires numerous analyses to derive an optimal busbar design. However, repetitive analyses reduce work efficiency. To address this issue, we have developed BeHAP, an automated busbar thermoelectric analysis program. We will introduce BeHAP and explain how to use it.

Introduction to busbars

As mentioned, busbars are used to transfer power between battery cells or modules. Functionally, they serve the same role as electrical wires.

As the cross-sectional area of copper increases, the current density decreases, which reduces the amount of heat generated.

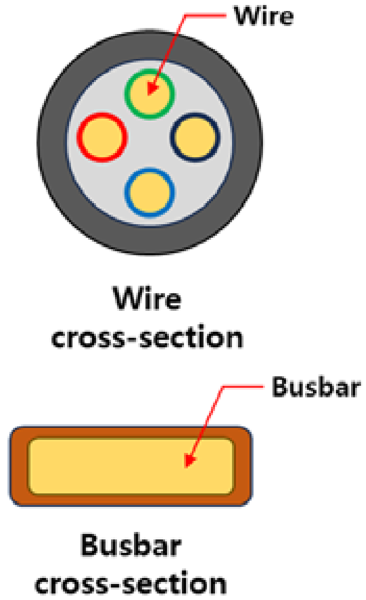

Fig. 1. Cross-section of wires and busbars.

These advantages help to manage heat generation and ensure structural stability against thermal deformation.

Joule-heating

To evaluate the heat generated by an electric current, a thermoelectric (joule-heating) analysis is required. It is also important to include the heat generation per unit volume in the numerical model. The formula is:

$$Q = \rho * J^2 \ [W/m^3]$$

The amount of heat generated per unit volume is calculated by multiplying the electrical resistivity (ρ) by the square of the current density (J). Electrical resistivity is a material property, while current density represents the amount of current flowing through a cross-section. In this case, the current value is a boundary condition specified by the user, meaning that the cross-sectional area is the final variable that determines the current density. Therefore, it follows that designers can improve the thermal management of busbars by modifying the cross-sectional area.

Thermoelectrical analysis process using Ansys

Before explaining how to perform a thermoelectric analysis using Ansys Mechanical, it is important to consider the systems that support the process. Ansys Workbench offers three analysis systems for thermoelectric analysis.

The first is a transient electrothermal coupled analysis. In this system, the current density is calculated in the electrical analysis. It is then imported into the thermal analysis as a boundary condition, after which the heat generation is calculated. The advantage of this configuration is that all boundary conditions supported by each analysis system can be used.

The second is thermoelectric analysis, which allows simultaneous calculation of current flow and heat generation within a single analysis system.

The third system is coupled field transient analysis. This calculates current density and heat generation over time, and can perform both electrothermal and electrothermal-structural analyses within a single system. It is ideal for users evaluating the structural stability of busbars based on thermoelectric effects, and is compatible with Ansys 2023R1 and later versions.

Of the analysis systems explained above, we will examine the overall thermoelectric analysis process of the busbar within the thermoelectric analysis system, and will introduce an automated program based on this process.

To perform the electrical analysis, boundary conditions such as current and voltage are set, as shown in Fig.2.

To numerically simulate the variation in current over time during battery charging and discharging, the current is inserted in profile format,

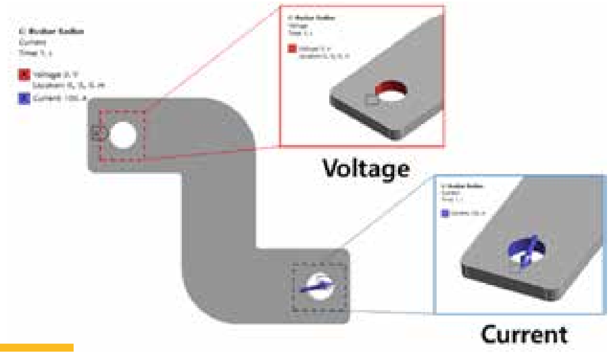

Fig. 2. Boundary conditions for electrical analysis.

Then, for the thermal analysis, the boundary and convection conditions are defined, taking into account the external environment, such as the ambient temperature and convection coefficient.

The boundary conditions are defined, and the analysis is performed to calculate results such as current density and temperature distribution.

Busbar joule-heating analysis program (BeHAP)

As explained above, the thermoelectric analysis is essentially a coupled electrical and thermal analysis, so it is performed in various environments. The process is as Fig. 3.

Fig. 3 shows how complicated the analysis workflow becomes as a result of the pre- and post-processing being performed in various environments, such as Workbench and Mechanical. The Busbar Joule-Heating Analysis Program (BeHAP) was developed to solve this problem.

The advantage of BeHAP is that pre- and post-processing can be performed simultaneously in a single environment. This simplifies the analysis workflow, making it accessible even to design engineers with limited analysis experience.

The BeHAP configuration screen consists of the Manual, Analysis Process, and Settings tabs. The Analysis Process tabs are organized in the following order: Modelling, Materials, Analysis Settings, and Results. Each step must be performed in sequence.

The Settings button allows users to check the status immediately by looking at the button colour. Yellow indicates that parts currently require configuration, while green indicates that configurations are complete. The colours allow users to verify the status of the settings within a step. Red indicates that an operation is in progress; white indicates unconfigured parts.

The first step in the analysis process in BeHAP is to set the Working Directory and Model. The Working Directory is the path that indicates where the project file (*.wbpj) is stored, while Model shows where the CAD file is loaded. CAD files are loaded via SCDM, meaning all design extensions supported by SCDM can be loaded.

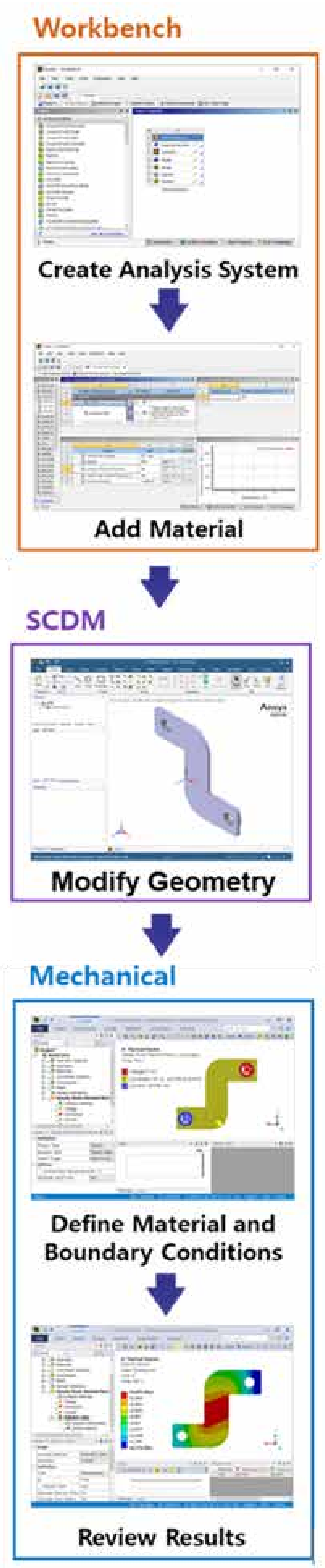

Fig. 3 Thermoelectrical analysis process in the Ansys environment.

Fig. 4. Thermoelectrical analysis process in BeHAP.

As shown in Fig.5, almost all busbar shapes are supported, including single-part models, multi-body parts consisting of several bodies, and assembly models composed of multiple busbars. After loading the CAD model, additional settings are required. Click the Start button on the screen to run SCDM and define the location of Current and Ground connections.

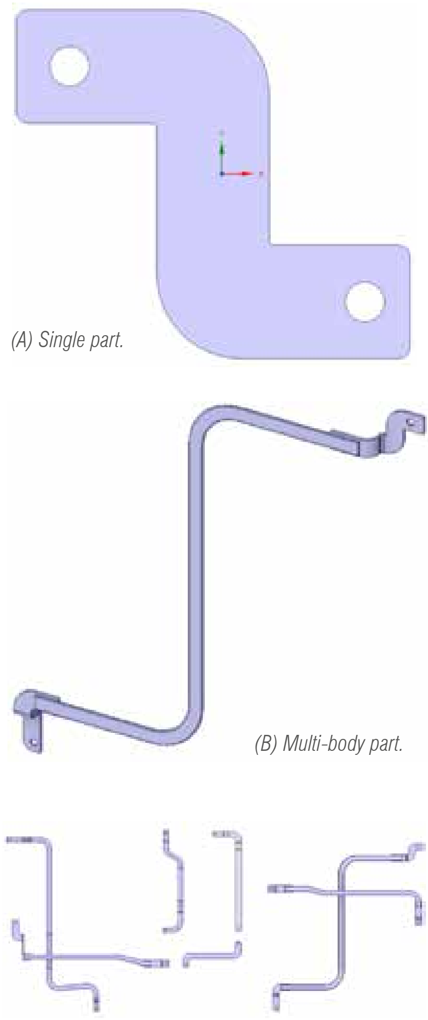

(A) Single part.

(B) Multi-body part.

(C) Assembly model.

Fig. 5. Busbar shape classification.

At this point, change the name of the part to which the current is applied to "Current," and change the name of the earthed part to "Ground."

Next, group the busbar line where electricity is generated, and its Current and Ground parts into one component. Then set the Share Topology option for that Component to Group.

Once all settings have been completed, exit SCDM. A popup window will then appear with the message "Settings complete" after which the user is automatically directed to the second step: the Materials tab.

The second step of the configuration process consists of a window in which the user checks, adds, and applies the properties for each part, as well as setting the contact resistance.

	Time [sec]	Current [A]
LS 0	0.0	300.0
LS 1	1200.0	300.0
LS 2	1200.1	500.0
LS 3	1500.0	500.0
LS 4	1500.1	400.0
LS 5	1800.0	400.0
LS 6	1800.1	350.0
LS 7	2200.0	350.0

(A) Current profile input table.

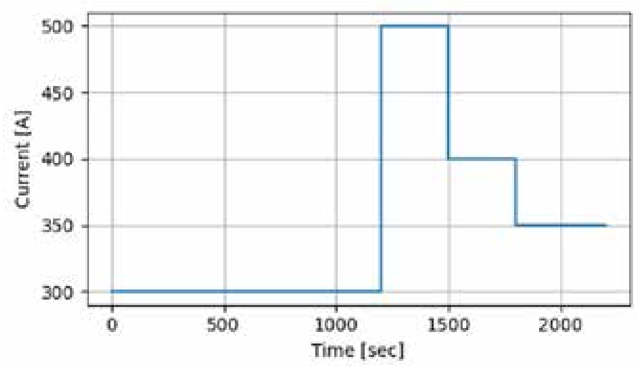

(B) Current profile graph.

Fig. 6. Setting of current profile.

The default material is copper (C1100), but the user can modify its properties. To use a different material, click on the Add Material button and enter a new property name, density, thermal conductivity, specific heat, and resistivity.

To assign material, click the Load Data button to load the list of parts list from the previously defined CAD file. Then apply the properties to each part and click the Apply button to save the data.

In addition, if contact resistance needs to be considered, this can be defined as well. By default, Ansys calculates the electrical contact conductance (ECC) value of the contact surface. However, if the user enters a value, the program will recalculate the ECC value based on the contact area and resistance, using this value in the analysis.

The third step is to set the analysis settings and boundary conditions.

First, select the type of analysis: steady-state or transient. If you want to see how temperature changes over time, choose transient analysis.

Next, set the initial temperature of the analysis. Thereafter, the ambient temperature and film coefficient must be defined to apply the convection conditions.

The number of CPU cores required for analysis can be specified, with four cores being offered as the default, but the maximum number that can be used depends on whether an HPC license is present.

Next, the current profile needs to be set. Inputs ranging from constant current to profiles where the current changes over time are all possible. As shown in Fig. 6, entering current values in the Current Profile tab will display a graph in the Current Profile Graph window to help prevent input errors.

Additionally, the program allows the user to load or save the current profiles using Excel. Current profiles loaded from Excel should be formatted as follows: Time in the first column, and Current Values in the second column.

The point at which the current value is entered is called the load step. If the time between two load steps is less than ten seconds, the previous load is divided into 10 sub-steps for better convergence. If the time exceeds ten seconds, sub-steps will be generated every ten seconds.

To adjust the number of sub-steps per load step, click the Optional Sub-step button and enter the desired number in the third column of the Current Profile table.

Once all settings have been completed, click the Solve button (shortcut key F5) to initiate the analysis. The button colour changes to green when the analysis is complete. The user then moves onto the final step, in the Results tab.

In the last step (Step 4), the Results tab is divided into two windows – one for checking the analysis results, and another for setting the plot options.

BeHAP allows users to choose to view temperature, and current density results as either a contour or a graph.

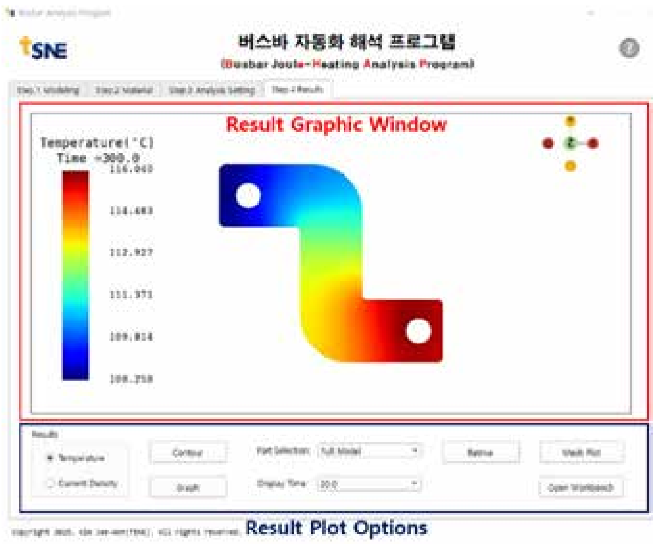

Fig. 7. Configuration screen for step 4.

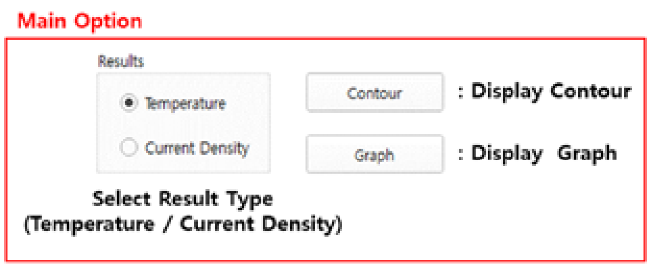

Fig. 8. Result plot - main option.

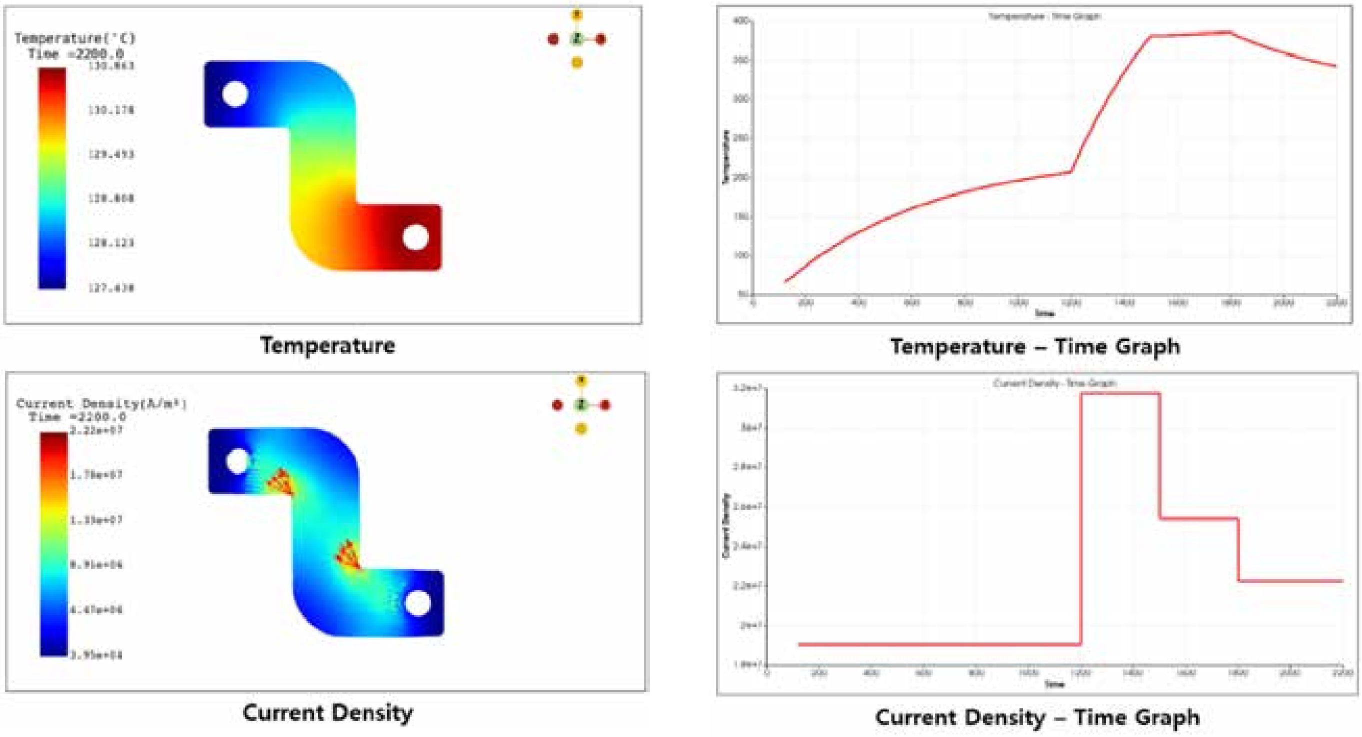

(A) Results as a contour.

(B) Results as a graph.

Fig. 9. BeHAP result output.

Clicking the Contour button, as shown in Fig. 9, displays the results of the last step. In the case of current density, the vector is also displayed. Results displayed via the Contour button can be shown in real time and checked in 3D. Clicking the Graph button, displays a graph of the results over time based on the highest temperature or maximum current density.

In the Detail option, users can view the results according to the selected settings and reissue them by selecting the Part and Time again. The Part setting allows users to check the results for a specific part but is only available when using the assembly model. The Time setting lets users set a time for each load step or sub-step. After selecting a Part and Time, click the Retrieve button to view the results.

Finally, users can check the grid shape using the Mesh Plot option. With Open Workbench, users can execute saved Workbench files to display additional results on the Ansys Mechanical screen.

Conclusion

This article discussed the thermoelectrical analysis process of busbars, which are power transmission components found in high-voltage batteries and introduced the Busbar Joule-Heating Analysis Program (BeHAP), which automates the pre- and post-processing.

We hope that the introduction of BeHAP, will allow you to work more efficiently, as it significantly reduces workload and time.

For more information:
Jae-won Kim - Taesung S&E
jwkim21@tsne.co.kr

About TSNE

Since its establishment in 1988, TSNE has specialized in CAE, providing engineering programs and services to Korean customers. Tae Sung S&E (TSNE) aims to be the "One Stop Total CAE Solution Provider" (OSTS) both in domestic and global markets. The company leverages its large base of business capabilities and its team of CAE experts to provide services to customers in various industries (aerospace, automotive, civil engineering, biomedical, shipbuilding, electrical and electronics, energy, defence, chemical industries, etc.) and is expanding its business scope to research innovative technologies and apply them in the field. It strives to become a global engineering company and increase its potential as a sustainable engineering company. Tae Sung S&E partners are all engineers who endeavour to solve challenges. Tae Sung S&E will work with you to achieve "NO PROBLEM, BE HAPPY


Enjoy our events
Meet our Experts
ENGINSOFT
Stay tuned
www.enginsoft.com/ourlatest
www.linkedin.com/company/enginsoft